



This is a repository copy of *Stochastic and global sensitivity analyses of uncertain parameters affecting the safety of geological carbon storage in saline aquifers of the Michigan Basin*.

White Rose Research Online URL for this paper:

<https://eprints.whiterose.ac.uk/86250/>

Version: Accepted Version

Article:

González-Nicolás, A., Baù, D., Cody, B.M. et al. (1 more author) (2015) Stochastic and global sensitivity analyses of uncertain parameters affecting the safety of geological carbon storage in saline aquifers of the Michigan Basin. *International Journal of Greenhouse Gas Control*, 37. 99 - 114. ISSN 1750-5836

<https://doi.org/10.1016/j.ijggc.2015.03.008>

Article available under the terms of the CC-BY-NC-ND licence (<https://creativecommons.org/licenses/by-nc-nd/4.0/>).

Reuse

This article is distributed under the terms of the Creative Commons Attribution-NonCommercial-NoDerivs (CC BY-NC-ND) licence. This licence only allows you to download this work and share it with others as long as you credit the authors, but you can't change the article in any way or use it commercially. More information and the full terms of the licence here: <https://creativecommons.org/licenses/>

Takedown

If you consider content in White Rose Research Online to be in breach of UK law, please notify us by emailing eprints@whiterose.ac.uk including the URL of the record and the reason for the withdrawal request.



eprints@whiterose.ac.uk
<https://eprints.whiterose.ac.uk/>

Stochastic and Global Sensitivity Analyses of Uncertain Parameters Affecting the Safety of Geological Carbon Storage in Saline Aquifers of the Michigan Basin

Ana González-Nicolás^{1*}, Domenico Baù^{1,2}, Brent M. Cody¹, Ayman Alzraiee¹

¹ Colorado State University, Civil and Environmental Engineering Department, Fort Collins, CO 80523-1372, USA

² Now at: University of Sheffield, Civil and Structural Engineering Department, Sheffield, S1 3JD, UK

*Corresponding author: T: +1-970-4037858

E-mail address: anagna@gmail.com (A. González-Nicolás)

Postal address: Colorado State University, Campus Delivery 1372, Fort Collins, CO 80523-1372, USA

Received 11 November 2014

Received in revised form 9 March 2015

Accepted: March 10, 2015

*REFERENCE: International Journal of Greenhouse Gas Control, Volume 37, June 2015, Pages 99–114.
doi:10.1016/j.ijggc.2015.03.008*

Abstract

Geological carbon storage (GCS) has been proposed as a favorable technology to reduce carbon dioxide (CO₂) emissions to the atmosphere. One of the main concerns about GCS is the risk of CO₂ escape from the storage formation through leakage pathways in the sealing layer. This study aims at understanding the main sources of uncertainty affecting the upward migration of CO₂ through pre-existing “passive” wells and the risk of fissuring of target formation during GCS operations, which may create pathways for CO₂ escape. The analysis focuses on a potential GCS site located within the Michigan Basin, a geologic basin situated on the Lower Peninsula of the state of Michigan. For this purpose, we perform a stochastic analysis (SA) and a global sensitivity analysis (GSA) to investigate the influence of uncertain parameters such as: permeability and porosity of the injection formation, passive well permeability, system compressibility, brine residual saturation and CO₂ end-point relative permeability. For the GSA, we apply the extended Fourier Amplitude Sensitivity Test (FAST), which can rank parameters based on their direct impact on the output, or first-order effect, and capture the interaction effect of one parameter with the others, or higher-order effect. To simulate GCS, we use an efficient semi-analytical multiphase flow model, which makes the application of the SA and the GSA computationally affordable. Results show that, among model parameters, the most influential on both fluid overpressure and CO₂ mass leakage is the injection formation permeability. Brine residual saturation also has a significant impact on fluid overpressure. While influence of permeability on fluid overpressure is mostly first-order, brine residual saturation’s influence is mostly higher-order. CO₂ mass leakage is also affected by passive well permeability, followed by porosity and system compressibility through higher order effects.

Keywords: CO₂ storage, semi-analytical algorithm, CO₂ leakage, fluid overpressure, parameter uncertainty, stochastic approach, global sensitivity analysis.

1 Introduction

The Earth's atmosphere is experiencing global climate change caused by increasing greenhouse gas concentrations. Carbon dioxide (CO₂) is the most important greenhouse gas produced by human activities (Solomon et al., 2007). In the last decade, geological carbon storage (GCS) has been identified as a promising technology for reducing CO₂ emissions to the atmosphere. Candidate storage formations include depleted oil and natural gas reservoirs, unmineable coal seams, and deep saline aquifers (Bergman and Winter, 1995; Ruether, 1998; Bachu, 2003). The latter represent potential alternatives to the lack of petroleum fields and constitute 60% of the estimated storage capacity worldwide (International Energy Agency, 2008). GCS in saline aquifers involves the injection of supercritical CO₂ into deep brine-saturated formations. Supercritical CO₂ is less dense and less viscous than the brine residing in saline formations, which causes gravity override as well as viscous fingering. Thus, supercritical CO₂ tends to migrate upwards driven by buoyancy unless low-permeable layers, or caprock, stop its vertical movement. However, if the injected CO₂ finds a potential leakage pathway through the caprock, it may adversely affect shallow fresh groundwater resources or even reach the land surface.

Sealing features of the caprock overlying the injected formations are critical elements for the effectiveness and safety of GCS operations. Nevertheless, unlike petroleum reservoirs, saline aquifers have never contained oil or gas. Consequently, there are less data associated with saline aquifers than petroleum reservoirs. In addition, information about the sealing properties of the caprock might be scarce or nonexistent. Typically, physical properties of potential candidate GCS sites are highly uncertain. Host rock permeability, spatial distribution of potential leakage pathways, and increase of fluid pressure in the injected formations may directly influence CO₂ leakage. Leakage pathways may also be created during the CO₂ injection process due to caprock fracturing associated with increased pore pressure and the ensuing reduction in effective stress. Therefore, assessing the risk of CO₂ leakage given the uncertainty on these parameters is vital prior to the implementation of GCS systems.

Carbon injection into deep saline aquifers involves complex processes of two-phase flow in confined geological formations, which make its modeling a demanding endeavor. Complexities associated with multiphase flow and transport processes, such as non-linearity, induced fingering and convective mixings, create the need for computationally efficient assessment approaches. Several analytical and semi-analytical solutions have appeared in the literature (e.g., Saripalli and McGrail (2002); Nordbotten et al. (2005a); Gasda et al. (2008); Dentz and Tartakovsky (2009); Vilarrasa et al. (2010); Mathias et al. (2011)), which rely on a number of simplifying assumptions. The main advantage of analytical and semi-analytical models is that they allow simulations to be performed in a very short central processor unit (CPU) time (of the order of seconds), which makes stochastic analyses (SAs) and global sensitivity analyses (GSAs) requiring on the order of thousands of model runs computationally viable.

Risk assessment is an important tool for decision making during the initial stages of GCS projects. Some algorithms have been developed to predict performance and risk of GCS systems (e.g., LeNeveu, 2008; Stauffer et al., 2008; Oldenburg et al., 2009; Dobossy et al., 2011), in which potential candidate sites are selected for evaluation of their safety and effectiveness. Several studies have been published that statistically analyze the uncertainty of leakage associated with parameters of the injected aquifer in a GCS system. For example, Celia et al. (2009) investigated the influence of the injection depth on leakage risk and showed that this risk decreases when injection depth increases.

CO₂ injection performance and sequestration efficiency have also been investigated. For example, Celia et al. (2011) found that CO₂ injection rates are reduced by higher brine residual saturations and are influenced by the relative permeability of CO₂. Gupta and Bryant (2011) found that more CO₂ trapping is achieved when the gravity number (*i.e.* the ratio between buoyancy and viscous forces) is low, leading to enhanced lateral displacement of the CO₂ plume. On the other hand, high gravity numbers lead to stronger gravity override, resulting in both less trapping of CO₂ and less contact between the CO₂ plume and ambient brine. Middleton et al. (2012) showed that uncertainties from permeability, porosity, and formation thickness significantly affect capacity and cost calculations.

Studies that analyze the uncertainty of leakage associated with abandoned wells can also be found. Kopp et al. (2010) conclude that increased risk of leakage is produced by a longer injection time, smaller distance between injection wells and leaky wells, higher permeability anisotropy, higher geothermal gradient, and shallower depth. In order to show that potential leakage depends on formation properties, as well as the location and the number of leaky wells, Nogues et al. (2012) conducted a Monte Carlo simulation where the main uncertainty was the effective well permeability.

Alternative methods for quantifying uncertainty by stochastic simulation can be found, for example, in the works of Oladyskin et al. (2011) and Walter et al. (2011). Both studies used an integrative probabilistic collocation method (Wiener, 1938; Li and Zhang, 2007) to reduce the computational cost associated with stochastic approaches. Specifically, Oladyskin et al. (2011) compared the probabilistic collocation method to a Monte Carlo approach as a risk assessment tool of CO₂ storage. Walter et al. (2011) used this method to study the pressure increase in a channel system during injection of CO₂.

Mathias et al. (2013) applied a local sensitivity analysis of permeability, porosity and relative permeability parameters based on data drawn from the literature on 25 formations. The sensitivity analysis addressed the impact of these parameters on the ratio between the CO₂ injection rate and the down-hole fluid overpressure –or injectivity– at the end of a prescribed injection period that is likely to cause fissuring of the formation. They showed that relative permeability parameters have a significant impact on aquifers of large extent, whereas the impact of compressibility and porosity is more important in “closed” compartmentalized aquifers. A local sensitivity analysis on the long-term behavior of CO₂ in a multilayered aquifer was conducted by Kano and Ishido (2011), who showed that, in the long-term, the most influential parameters are geothermal gradient, layer thicknesses, capillary pressure, relative permeability and permeability. Aoyagi et al. (2011) presented an example of a local sensitivity analysis of productivity index and fault permeability affecting the leakage of CO₂ through wells or faults. They found that the fault permeability value is more relevant when leakage starts. Zhao et al. (2010) determined that

CO₂ dissolution increased when the vertical-to-horizontal permeability ratio, critical gas saturation, or brine salinity are decreased, and when brine saturation is increased.

GSA (Saltelli, 2008) differs from the local sensitivity analysis in that GSA explores the whole parameter space and is able to rank parameters according to their importance. GSA methods include methods such as Fourier amplitude sensitivity test (FAST) (Cukier et al., 1978; Saltelli et al., 1999; Saltelli, 2008), Morris analysis (Morris, 1991), and Sobol's indices (Sobol', 2001). These last two methods have been applied recently by Wainwright et al. (2013) to investigate the complementarity of GSA and local sensitivity analysis in a hypothetical GCS site located in the Southern San Joaquin Basin in California, USA. Another option to compute sensitivity measures when observations are available is the Generalized Likelihood Uncertainty Estimation (GLUE) (Beven, 1993). One example of the use of GLUE to produce sensitivities measures for each parameter based on Kolmogorov–Smirnov statistic can be found in McIntyre et al. (2005).

All these studies investigate uncertainties of multiple factors to aid the decision making of best injection strategies. The aim of this study is to provide an understanding of the main sources of uncertainty that affect leakage through potential escape pathways and fluid overpressure variability, thereby identifying where data collection efforts should be directed to improve the characterization of a candidate site for GCS. With this purpose, we conduct SAs and GSAs to investigate the effect of several parameters –such as permeability and porosity of injection formations, passive well permeability, system compressibility, brine residual saturation and CO₂ end-point relative permeability – on (i) the maximum fluid overpressure produced by carbon injection and (ii) the mass of CO₂ that migrates into overlying formations through passive wells in relation to the total mass of injected CO₂. The main goal of the SA is to estimate the probability of fracturing the caprock, and the probability of leaked mass to exceed predefined threshold values. In carrying out the GSA, we apply the extended FAST method (Saltelli et al., 1999), which captures not only the uncertain parameters having more influence on the model output, but also the interaction effect among these parameters. In all analyses, CO₂ injection is simulated using ELSA-IGPS, a semi-analytical model developed by Cody et al. (2014), which builds upon the semi-

analytical solution of Celia and Nordbotten (2009) and Nordbotten et al. (2009). These analyses focus on a potential GCS site embedded in the Michigan Basin.

This paper is organized as follows. First, the multiphase flow model is presented, followed by a description of the methodologies used for stochastic analysis and global sensitivity analysis. Results of the application of these methodologies to the Michigan Basin test site are thus presented and discussed. Last, a summary and conclusions of this work are given.

2 Multiphase Flow Semi-Analytical Model

The algorithm used in this study is called ELSA-IGPS (Estimating Leakage Semi-Analytically-Iterative Global Pressure Solution) (Cody et al., 2014), and constitutes a modified version of the semi-analytical model ELSA devised by Celia and Nordbotten (2009) and Nordbotten et al. (2009).

By solving the partial differential equations for two-phase immiscible flow, Nordbotten et al. (2005b) developed a semi-analytical solution to estimate the leakage of brine and CO₂ flux through permeable caprock locations resulting from GCS. In ELSA-IGPS, the domain is structured into a stack of L aquifers separated by $L + 1$ caprock layers, perforated by M carbon injection wells and N passive wells. The model relies on the following assumptions:

- Permeable caprock locations are segments of pre-existing, abandoned wells and represent cylindrical portions of the caprock layers having low, yet non-negligible, permeability. These are referred to as “passive” wells and are assumed to be the only pathways for fluid flux exchange between permeable layers. Consequently, diffusion leakage across the caprock is neglected.
- Aquifers are assumed to be horizontal, homogenous, isotropic, and permeable formations of large, virtually infinite, extent, confined between impervious top and bottom layers.
- Initially, fluid is not flowing through any of the passive wells as the entire domain is assumed saturated with brine under hydrostatic-pressure conditions.
- Flow is perfectly horizontal.

- Dissolution and chemical reactions are neglected since the time scale at which these processes occur (centuries and millennia, respectively) is much greater than the time scale of the injection operations (decades) considered for this study.
- Capillary pressure is neglected; therefore CO₂ and brine pressures at the interphase are equal.
- Pressure response from sources and sinks can be superimposed in each aquifer.
- The CO₂ plume thickness at any given location is the effect of all CO₂ sources and sinks in the aquifer. For any position where there is an overlap of CO₂ plumes, CO₂ saturations are calculated by assuming the maximum plume thickness. This must lead to a loss of CO₂ mass in the system.
- Injection wells are theoretically able to inject into any of the L aquifers.
- CO₂ injection is constant during the injection period, even for low permeability formations, and no post-injection phase is simulated.

Due to its significant amount of assumptions, this solution is adequate for pre-screening and risk analyses but not recommended for supporting the final design of GCS systems.

ELSA-IGPS, as the original model, applies superposition of effects for the fluid flux across sources iw (injection wells, $iw=1,2,\dots,M$) and sinks j (passive wells, $j=1,2,\dots,N$) to solve the fluid pressure $p_{j,l}$ [ML⁻¹T⁻²] at any given time t [T] at the bottom of the generic aquifer l ($l=1,2,\dots,L$) and for each passive well j . Therefore, fluid pressure can be expressed as:

$$p_{j,l} = p_{0l} + (\rho_b - \rho_c)gH_l[\sum_{iw=1}^M \Delta p'(\chi_{iw,j,l}) + \sum_{i=1}^N \Delta p'(\chi_{i,j,l})] \quad (1)$$

where: p_{0l} is the initial fluid pressure [ML⁻¹T⁻²] at the bottom of the aquifer l , ρ_α is the fluid density [ML⁻³] (α denotes the phase type, b for brine and c for CO₂), g is the gravitational acceleration [LT⁻²], H_l is the aquifer thickness [L] of aquifer l , and:

$$\Delta p'(\chi) = \begin{cases} 0 & \text{for } \chi \geq \psi \\ -\frac{1}{2\Gamma} \ln\left(\frac{\chi}{\psi}\right) + \Delta p'(\psi) & \text{for } \psi > \chi \geq 2\lambda \\ \frac{1}{\Gamma} - \frac{\sqrt{\chi}}{\Gamma\sqrt{2\lambda}} + \Delta p'(2\lambda) + F(h') & \text{for } 2\lambda > \chi \geq \frac{2}{\lambda} \\ -\frac{1}{2\lambda\Gamma} \ln\left(\frac{\chi\lambda}{2}\right) + \Delta p'\left(\frac{2}{\lambda}\right) & \text{for } \frac{2}{\lambda} > \chi \end{cases} \quad (2)$$

where:

$$\chi = \frac{2\pi H\varphi(1-s_b^{res})r^2}{Qt} \quad (3)$$

$$\Gamma = \frac{2\pi(\rho_b - \rho_c)gkH^2}{\mu_b Q} \quad (4)$$

$$\psi = \frac{4.5\pi H\varphi k(1-s_b^{res})}{\mu_b c_{eff} Q} \quad (5)$$

$$h' = \frac{h(\chi)}{H} = \frac{1}{\lambda-1} \left(\frac{\sqrt{2\lambda}}{\sqrt{\chi}} - 1 \right) \quad (6)$$

$$F(h') = \frac{-\lambda}{\lambda-1} \left[h' - \frac{\ln[(\lambda-1)h'+1]}{\lambda-1} \right] \quad (7)$$

where: h is the CO₂ plume thickness [L]; h' ['] is the CO₂ plume thickness relative to the aquifer thickness H ; s_b^{res} is the residual saturation of the brine [']; k is the aquifer permeability [L²]; μ_b is the dynamic viscosity of the brine [ML⁻¹T⁻¹]; φ is the aquifer porosity [']; Q is the total volumetric well flux [L³T⁻¹]; c_{eff} is the effective compressibility of the fluid and solid matrix [M⁻¹LT²]; and r is the radial distance [L]. $F(h')$ is an offset term related to the vertical pressure distribution (Celia et al., 2011) and the mobility ratio λ [']. The mobility ratio is defined as $\lambda = \lambda_c/\lambda_b$, where $\lambda_\alpha = k_{r,\alpha}/\mu_\alpha$ and $k_{r,\alpha}$ is the relative permeability of phase α . The $k_{r,b}$ is equal to one in areas where the CO₂ plume has not reached, since the brine saturation is equal to one. In areas that have been invaded by the CO₂ plume, the $k_{r,c}$ is given by the end-point CO₂ relative permeability $k_{r,c0}$, which depends on s_b^{res} . The effective compressibility of the fluid and solid matrix is defined as (Nordbotten et al., 2009):

$$c_{eff} = \left[\frac{1-s_b^{res}}{\rho_c} \frac{\partial(\varphi\rho_c)}{\partial p} + \frac{s_b^{res}}{\rho_b} \frac{\partial(\varphi\rho_b)}{\partial p} \right] \cong \frac{1}{\rho_b} \frac{\partial(\varphi\rho_b)}{\partial p} \quad (8)$$

c_{eff} is assumed to be equal to the brine compressibility since the domain is mostly filled with brine.

This derives to a system of equations where the unknowns are the fluid pressures $p_{j,l}$ at the bottom of each aquifer l and at each passive well j , and the flow rates $Q_{j,l}$ across each caprock for each passive well. $Q_{j,l}$ is calculated using the multiphase version of Darcy's law:

$$Q_{j,l} = \sum_{\alpha=b,c} \left[\pi r_{pw,j,l}^2 \frac{k_{r,\alpha,j,l} k_{pw,j,l}}{\mu_\alpha B_l} (p_{j,l-1} - \rho_\alpha g B_l - g \rho_\alpha H_{l-1} - p_{j,l}) \right] \quad (9)$$

where: $r_{pw_{j,l}}$ is the passive well radius [L], $k_{r,\alpha_{j,l}}$ is the relative permeability of phase α [/], and $k_{pw_{j,l}}$ is the single phase passive well permeability [L²] for passive well j and aquitard layer l , and B_l is the caprock thickness [L] for aquitard layer l .

The fluid pressure (Equation 1) at the bottom of each aquifer and at each passive well can be grouped into a $(N \cdot L) \times 1$ vector. Similarly, the flow rates (Equation 9) across each aquitard for each passive well can be grouped into another $(N \cdot L) \times 1$ vector. By combining these two vectors a set of $2 \cdot N \cdot L$ non-linear equations with $2 \cdot N \cdot L$ unknowns is obtained. Domains having large numbers of passive wells (N) and/or layers (L) produce very large sets of equations; resulting in significantly higher simulation run times. To solve this system of non-linear equations at a time t , a computational efficient fixed-point iterative scheme (Takahashi, 2000) is developed. For more details about ELSA-IGPS, the reader is referred to (Cody et al., 2014). The ELSA-IGPS algorithm (Cody et al., 2014) allows for drastically reducing the computational effort (a complete simulation takes CPU times on the order of seconds or minutes) making possible the application of this solution within a stochastic simulation (or Monte Carlo) approach or a global sensitivity analysis such as those described in the following sections. In this study, ELSA-IGPS is used to explore the uncertainty and sensitivity of the input parameters on the uncertainty and variability of two states variables of interest: i) the fluid overpressure nearby the injection well, and ii) the percentage of CO₂ mass leakage into overlying formations. Fluid overpressure Δp_{iw} is defined as the difference between the final (at final time t_{end}) and initial fluid pressures in proximity of the injection well. In our analyses, the number of injection wells M is set equal to 1, and injection occurs into the deepest aquifer ($l=1$). Therefore, based on Equation (1), the fluid overpressure nearby the injection well at final time is calculated as:

$$\Delta p_{iw} = \Delta p_{1,1}(r'_{iw}, t_{end}) = (\rho_b - \rho_c)gH_1[\Delta p'(\chi_{1,1,1}) + \sum_{i=1}^N \Delta p'(\chi_{i,1,1})] \quad (10)$$

where r'_{iw} is a radial distance nearby the injection well. The total CO₂ mass leakage is given by:

$$M_{leak}(t_{end}) = \int_0^{t_{end}} [\sum_{i=1}^N \rho_c S_{c,i,2}(\tau) Q_{i,2}(\tau)] d\tau \quad (11)$$

where $s_{c,i,2}$ is the CO₂ saturation at passive well i and layer $l=2$. Thus, the percent of CO₂ mass leakage $\%M_{leak}$ is defined as the ratio between the mass of CO₂ that escapes from the injected aquifer into overlying formations and the total mass of injected CO₂ at time t_{end} :

$$\%M_{leak} = \frac{M_{leak}(t_{end})}{\rho_c Q_{i,1} t_{end}} 100 \quad (12)$$

3 Stochastic Analysis

Stochastic, or Monte Carlo, simulation is a mathematical method that allows for the analysis of complex systems while accounting for uncertainty in quantitative terms. Values of the uncertain parameters are sampled randomly from their respective probability distribution functions (PDF), which are meant to reproduce the uncertainty of the parameter. In the stochastic analysis (SA) presented here, the uncertain input parameters that may affect the state variables of interest, that is, Δp_{iw} (Equation 10) and $\%M_{leak}$ (Equation 12) are: permeability and porosity of injection formations, passive well permeabilities, system compressibility, brine residual saturation and the CO₂ end-point relative permeability. These uncertainties are modeled conceptually using a series of independent PDFs representing typical ranges of parameter uncertainty. In the case of passive well permeability, three PDFs are considered. Ensembles of uncertain parameters are used within the mathematical model (see Section 2) to simulate how parameter uncertainty affects the uncertainty in the state variables of interest. Output ensembles of the state variables are used to produce cumulative distribution function (CDF) plots. The CDF of the generic state variable Y , either Δp_{iw} or $\%M_{leak}$, is obtained from the output of N_{MC} model simulations, where N_{MC} is the size of the ensemble. After ordering the Y values in ascending order, $Y_1 < Y_2 < \dots < Y_{N_{MC}}$, the corresponding CDF values are calculated as $CDF(Y) = (i - 0.5)/N_{MC}$ ($i=1,2,\dots,N_{MC}$) (Hahn, 1967). By analyzing the statistics of the output ensembles ($Y_1 < Y_2 < \dots < Y_{N_{MC}}$) the information that can be drawn is, for example, PDF type and its parameters, ensemble spread, quantiles, confidence bounds, and percentile values. In the case of state variables such as Δp_{iw} (Equation 10) and $\%M_{leak}$ (Equation 12 (12)), percentile values can be used to estimate the probability of

fracturing the caprock formations and the probability of leaked mass to exceed predefined threshold values.

4 Global Sensitivity Analysis

In this study, we apply the extended FAST introduced by Saltelli (1999). Extended FAST is a GSA variance-based method, which allows ranking input parameters according to its importance. In addition, extended FAST method allows uncovering the interaction among different parameters (higher order sensitivity index) and its contribution to prediction uncertainty, a situation that cannot be achieved with typical sensitivity analyses or stochastic simulation. Therefore, extended FAST improves the understanding of the complex dynamics between input parameters and output prediction. This understanding might be exploited, for example, to perform post-GSA uncertainty analyses, in which uncertainty is restricted to the most important parameters obtained with the extended FAST analysis, and to guide data collection and focus limited resources on the most sensitive parameters.

For each uncertain parameter Z_i , the extended FAST method provides two sensitivity measures: the first-order index and the total effect index. The first-order index S_i represents the main effect contribution of each model input parameter Z_i to the variance of the generic model output Y (Δp_{iw} or $\%M_{leak}$). In practice, S_i quantifies how much the variance of Y would be reduced if the uncertain input parameter Z_i was fixed. This index is calculated as (Saltelli, 2008):

$$S_i = \frac{V[E(Y|Z_i)]}{V(Y)} \quad (13)$$

where $V(\cdot)$ indicates the variance operator and $E(Y|Z_i)$ indicates the expected value of Y conditioned to Z_i , and $V[E(Y|Z_i)]$ is the first-order effect.

Two or more input parameters present interaction when the sum of their first-order indices cannot explain their effect on Y . $V(Y)$ can thus be decomposed into first-order and higher-order effect terms:

$$V(Y) = \sum_{i=1}^n V_i + \sum_{i=1}^n \sum_{j=i+1}^n V_{ij} + \sum_{i=1}^n \sum_{j=i+1}^n \sum_{l=j+1}^n V_{ijl} + \dots \quad (14)$$

where $V_i = V[E(Y|Z_i)]$ is the first-order effect of Z_i , and $V_{ij} = V[E(Y|Z_i, Z_j)] - V[E(Y|Z_i)] - V[E(Y|Z_j)]$ is the second-order effect between parameters Z_i and Z_j , etc. It is possible to show that the total number of terms at the right-hand side of Equation (14) is $2^n - 1$, which increases exponentially with n . This makes the calculation of higher-order indices computationally intensive. As an alternative to compute higher-order indices, GSA computes the total effect index S_{T_i} ($i=1,2,\dots,n$), which detects the interaction of the parameter Z_i with all other parameters and represents its total contribution to the model output. In other words, S_{T_i} is equal to the first-order index S_i plus the interaction of Z_i with other uncertain parameters, and is calculated as (Saltelli, 2008):

$$S_{T_i} = 1 - \frac{V[E(Y|\mathbf{z}_{\sim i})]}{V(Y)} \quad (15)$$

where $\mathbf{z}_{\sim i}$ is the vector including all input parameters but Z_i . Consequently, the sum of higher-order effects S_{I_i} ($i=1,2,\dots,n$) can be defined as $S_{I_i} = S_{T_i} - S_i$. The index S_{I_i} quantifies the importance of the interaction of parameter Z_i with the all other input parameters. Consequently, if S_{I_i} is negligible, then the interaction of the uncertain parameter Z_i with other parameters is non-relevant ($S_{I_i} \approx 0$ and $S_{T_i} \approx S_i$). On the other hand, the value of S_{T_i} provides information concerning the relevance of the input parameter Z_i . If S_{T_i} is zero or close to zero, then the parameter Z_i can be set to any value of its range of variability without having any impact on the output variance of the model.

Extended FAST is a Monte-Carlo based numerical procedure, where the variances and the conditional variances of the model response with respect to uncertain input parameters are estimated from the output of an ensemble of model runs. To apply the extended FAST and compute first-order and total effect indices of each parameter the SIMLAB package (SIMLAB, 2007) is employed. The total number of executions that the extended FAST method requires is equal to $D(2 + n)$, where D is the size of the ensemble used for each input parameter, which can range from a few hundreds to a few thousands. For example, for a number of 5 input parameters and an ensemble size of 1,000, extended FAST would require 7,000 runs. Inevitably, for a model with a large number n of input parameters, this method

requires large ensembles of executions, and is viable only for simulation models that are not computationally intensive, as is the case of the multiphase flow simulator presented in Section 2.

5 Application to the Michigan Basin Test Site

5.1 Site description

The SA and GSA introduced in Sections 3 and 4 are applied to a geological test site located near the town of Thompsonville, MI. The storage formation proposed for GCS is embedded in the northern reef trend of the Michigan Basin. These reefs are evaporate-encased and, up until a few decades ago, significantly contributed to the production of hydrocarbons in Michigan. Most of these formations are associated with the reef buildups of Middle Silurian age. Figure 1 shows a cross-section of the Michigan Basin in the area of interest with available log-wells. The Gray Niagaran formation, highlighted in yellow, lies below the Brown Niagaran pinnacle, a depleted oil reservoir currently used by Michigan Technological University for geophysical research (Figure 1). This formation is chosen as a candidate to store supercritical CO₂ because it lies underneath the Brown Niagaran pinnacle, and thus the sealing capacity in that region is almost certainly assured. In addition, the Gray Niagaran formation is already perforated by two exploration wells (Burch 1-20B and Stech 1-21A), which could possibly serve as CO₂ injection wells. The top and the bottom of this formation lie at a depth of 1,500 m and 1,619 m below ground, respectively. These characteristics make this formation a good candidate for storage of CO₂ in supercritical state.

[Figure 1 here]

Figure 1. Cross-section of the Michigan Basin test site (adapted from Turpening et al. (1992)). The Gray Niagaran formation highlighted in yellow, is selected as potential candidate for GCS.

The information available on the Gray Niagaran formation in the Michigan Basin indicates that no lateral boundaries are present within the regions affected by fluid pressure variations due to GCS during the considered simulation periods. Therefore the assumption of infinite lateral boundary can be assumed as valid in the analyses. To simplify the simulation of CO₂ injection, the system is modeled as an aquifer (the Gray Niagaran formation) confined by one sealing caprock (Evaporites), and another aquifer with lower permeability (Carbonate formation) located above the sealing caprock. Supercritical CO₂ is injected within the lower aquifer from a single well. The thicknesses of the Gray Niagaran formation and the overlying aquifer are 119 m and 35 m, respectively. The caprock has a thickness of 17 m and is assumed impermeable except where there are passive wells. The area of interest covers a horizontal extent of about 9,000 m × 9,000 m around the Brown Niagaran pinnacle and comprises a total of 80 potentially leaky wells drilled across the Gray Niagaran formation. The locations of these wells have been obtained from the Michigan Department of Environmental Quality Oil and Gas Database (MDEQOGD, 2014). If these wells are deteriorated or not well cemented, they may represent a pathway for upward leakage of both brine and CO₂ from the Gray Niagaran formation. In this study, all formations are assumed initially saturated with brine under hydrostatic pressure conditions.

In the analyses presented here, a reference case is considered with the hydro-geomechanical parameters provided in Table 1. Wells logs (SCH, 1983; Halliburton, 1990; SCH, 1991) are available for the two boreholes shown in Figure 1. Log-porosity values are extracted from neutron porosity hydrogen index from the available logs. Given the lack of data, permeabilities k , in millidarcy (mD; $1\text{mD} \equiv 1 \times 10^{-15} \text{m}^2$), for the candidate formation and the overlying aquifers are estimated from porosity φ as (Trebin, 1945):

$$k = 2e^{31.6\varphi} \quad \text{if } 100\varphi < 12\% \quad (16)$$

$$k = 4.94(100\varphi)^2 - 763 \quad \text{if } 100\varphi > 12\%$$

Table 1. Hydro-geomechanical parameters of the reference case. Parameters of this table remain unchanged (deterministic) unless the parameter of interest is considered uncertain.

[Table 1 here]

These relationships have been deemed fairly adequate for low porosity reservoir rocks, carbonates and sandstones (Aschenbrenner and Chilingar, 1960), and are used here to assign permeability values of k_1 and k_2 in the reference case (see Table 1). The relative permeabilities of CO₂ and brine at the passive wells are calculated using the Van Genuchten model (Van Genuchten, 1980), with a fitting parameter of 0.41 and a brine residual saturation equal to 0.3 (Zhou et al., 2009). The brine residual saturation at the injection formation, s_b^{res} , is assumed to be equal to 0.3 for the reference case of Table 1.

In this study, fluid properties, density and viscosity, of CO₂ and brine are considered constant and independent of pressure and temperature. The effects of variability in fluid properties have also been commented in works of Celia and Nordbotten (Nordbotten et al., 2005a; Nordbotten and Celia, 2006; Celia and Nordbotten, 2009), who indicated that changes in these fluid properties are not important when CO₂ injection occurs for pressures and temperatures much greater than CO₂ critical point. The depth of the injection formation (below 1,500 m) assures that pressure and temperature are beyond the critical point. The radial distance r'_{iw} , where the fluid overpressure is evaluated, is equal to 5 m. The choice of such value is driven by considerations on the accuracy of the semi-analytical model, which is likely to give unreliable results for smaller distances, where high pressure gradients make the system divert significantly from the conditions of laminar flow required to apply Darcy's law. Previous calculations indicate that using values of the parameters in Table 1 and for average pore size values of the order of 5 μm , which are considered realistic for the investigated site, Reynolds' numbers for laminar flow are easily exceeded at radial distances less than 5 meters.

The uncertain parameters of interest are: permeability k_1 and porosity φ_1 of the injection formation, passive wells permeability k_{pw} , system compressibility c_{eff} , and brine residual saturation s_b^{res} . A PDF is prescribed for each of these parameters to represent their uncertainty for the candidate formation. These PDFs are given in Table 2. Note that permeability k_1 and porosity φ_1 are treated as

independent stochastic variables during the analyses and Equation (16) is only used to estimate the median value of the k_1 PDF. Thus permeability k_1 follows a lognormal PDF with a median permeability of $2.8 \times 10^{-14} \text{ m}^2$ and a log-standard deviation of 0.5 log-m^2 . Porosity φ_1 follows a uniform PDF with minimum and maximum values of 0.05 and 0.35 respectively. To characterize the permeability of passive wells, three different PDFs sharing the same median (*i.e.* the mean in the log-transformed space) are considered (see Table 2). In Case 1, a lognormal PDF with a median permeability of $1.0 \times 10^{-14} \text{ m}^2$ and a log-standard deviation of 1 log-m^2 is adopted (Nordbotten et al., 2009). For Cases 2 and 3, binary distributions are assigned, in which each passive well permeability may assume two values corresponding to a well-sealed passive well and to a leaky passive well, each with a 50% probability of occurrence. In Case 2, the value of permeability assigned to well-cemented passive well is $1 \times 10^{-17} \text{ m}^2$ (corresponding to the minimum value in Table 2), and the value of permeability assigned to a poorly cemented passive well is $1 \times 10^{-11} \text{ m}^2$ (corresponding to the maximum value in Table 2). In Case 3, the permeabilities for a well-cemented well and a leaky passive well are $1 \times 10^{-16} \text{ m}^2$ and $1 \times 10^{-12} \text{ m}^2$, respectively. In both cases, the permeability corresponding to a cemented well never exceeds the maximum permeability recommended for a well-sealed passive well, which is $2 \times 10^{-16} \text{ m}^2$ according to Kutchko et al. (2009). The PDFs of Case 1, Case 2, and Case 3 are shown in Figure 2. System compressibility c_{eff} follows a lognormal PDF with median equal to 4.6×10^{-10} and a log-standard deviation of 1 log-Pa^{-1} . Brine residual saturation is represented by a uniform PDF with a minimum value of 0 and a maximum value of 0.6.

Table 2. Probability distribution functions (PDFs) for uncertain parameters.

[Table 2 here]

[Figure 2 here]

Figure 2. PDFs of passive well permeability assigned to Case 1, Case 2, and Case 3. Details of these PDFs are in Table 2.

The residual brine saturation s_b^{res} is implicitly related to the CO₂ relative permeability $k_{r,c}$ and affects its “end-point” value at the brine residual saturation, $k_{r,c0}$. To account for this dependency, for each s_b^{res} value considered in the analyses, a $k_{r,c0}$ is introduced. Since there are no data available for the GSC candidate formation at hand, data from the literature are used to derive a statistical correlation between s_b^{res} and $k_{r,c0}$. While $k_{r,c0}$ is considered uncertain in our analyses, its impact on the model outputs is not addressed explicitly. For this purpose, s_b^{res} and $k_{r,c0}$ data corresponding to carbonate/dolomite formations are retrieved from the works of Bennion and Bachu (Bennion and Bachu, 2008; Bennion and Bachu, 2010). With these data, a non-linear exponential regression between s_b^{res} and $k_{r,c0}$ is hypothesized:

$$\overline{k_{r,c0}} = e^{-as_b^{res}} \quad (17)$$

where a is the coefficient obtained by running the exponential regression, and $\overline{k_{r,c0}}$ is the median value of $k_{r,c0}$. Also, a half amplitude confidence interval for $k_{r,c0}$ is calculated and applied around $\overline{k_{r,c0}}$:

$$k_{r,c0}^{\pm} = e^{-as_b^{res} \pm 4\delta s_b^{res}(1-s_b^{res})} \quad (18)$$

where δ is the standard deviation of the natural-log transformed $k_{r,c0}$ data. Substitution of Equation (17) into Equation (18) results in:

$$k_{r,c0}^{\pm} = \overline{k_{r,c0}} \cdot e^{\pm 4\delta s_b^{res}(1-s_b^{res})} \quad (19)$$

Therefore in the analyses, as s_b^{res} is sampled from the uniform PDF given in Table 2, $k_{r,c0}$ is generated as $k_{r,c0} = \overline{k_{r,c0}} \cdot e^{z \cdot s}$, where $s = 4\delta s_b^{res}(1 - s_b^{res})$ and z is a randomly generated value fitting to a standard normal PDF. Figure 3 represents the of $k_{r,c0}$ and s_b^{res} data obtained from Bennion and Bachu (Bennion and Bachu, 2008; Bennion and Bachu, 2010) together with the exponential regression and the half amplitude confidence intervals.

[Figure 3 here]

Figure 3. Representation of $k_{r,c0}$ and s_b^{res} data of carbonates/dolomites (Bennion and Bachu, 2008; Bennion and Bachu, 2010), exponential regression (in black), and the half amplitude of confidence interval (in grey).

Preliminary tests are run to estimate the minimum ensemble size beyond which CDFs remain substantially stationary. Based on the results of these tests sample sizes of $N_{MC}=1,000$ and $D=1,000$ are selected for the SA and the GSA, respectively.

In the SA, the 80 passive wells are considered individually in the semi-analytical model. In the GSA, these wells are clustered into 20 equivalent leakage pathways. Clustering of the 80 passive wells reduces the number of input parameters n in the GSA, which includes four system parameters (permeability k_1 and the porosity φ_1 of the injection formation, compressibility c_{eff} , and brine residual saturation s_b^{res}) and the permeabilities of 80 passive wells. Consequently, the computational cost of the extended FAST procedure (which requires $D(2 + n)$ model simulations, see Section 4) is reduced from $1,000 \times (2+84)=86,000$ to $1,000 \times (2+24)=26,000$ after well clustering. This clustering is performed by an optimization procedure that minimizes the sum of the Euclidean distances of the passive wells forming a cluster and the cluster centroid. When the cluster configuration is identified, each cluster of wells is substituted by an “imaginary” well located on the cluster centroid and having an equivalent circular area given by the sum of the cross-section areas of the passive wells within the cluster. From the cluster equivalent area a radius is derived and used in Equation (9) to calculate flow rates through them. The clustering of passive wells is not expected to affect significantly the results of the GSA. The presence of passive wells has little influence on fluid pressure at the injection well and thus the impact of passive-well clustering on this state variable is negligible, unless these wells were located in close proximity of the injection units. On the other hand, the intensity of CO₂ mass leakage might be affected by clustering, since it depends on the distances of the passive wells from the injection well. However, when clustering is applied, the increased leakage associated with the passive wells that are “moved” closer to the injection

well, is somehow offset by the decreased leakage associated with the passive wells that are “moved” away from the injection well. For this reason, the difference of CO₂ mass leakage due to the clustering can be assumed negligible.

Figure 4 shows the position of the 80 passive wells (MDEQOGD, 2014) located in the area under consideration and the position of each cluster of wells. The GSA is applied to study the impact of these 24 parameters on the maximum fluid overpressure reached around the injection well Δp_{iw} (Equation 10) and on the percent of CO₂ mass leakage $\%M_{leak}$ (Equation 12). The input parameters are characterized by the PDFs given in Table 2. With regard to passive well permeability, this follows the PDF of Case 1 according to results of Section 5.2.2.

[Figure 4 here]

Figure 1. Location of the 80 passive wells (indicated as crosses) that reach the Niagaran formation and location of the 20 equivalent leakage pathways (indicated as circles) used in the GSA and obtained after clustering the 80 passive wells. The injection well is located at the center of the domain.

5.2 Results and discussion

This section includes first a preliminary analysis carried out to select the CO₂ injection rate and the duration of CO₂ injection. Next, we present and discuss the results of the SA and the GSA for the Michigan Basin deep saline aquifer introduced in Section 5.1.

5.2.1 Selection of CO₂ injection rates

To choose an appropriate injection rate, a set of multiphase flow simulations is performed for a hypothetical system representative of the Michigan Basin. This hypothetical system consists of the same permeable formations and caprock considered for this study plus two overlying aquifers of thickness equal to 37 m and 75 m, underlain by two 18-m and 109-m thick aquitards, corresponding to the formations illustrated in Figure 1. Deterministic values of porosity are assigned to each layer based on

values from available log-wells (SCH, 1983; Halliburton, 1990; SCH, 1991). Permeability values are calculated with Equation (17). The aquifers are named L1, L2, L3 and L4, from the deepest to the shallowest. Aquitards are assumed impermeable except where passive wells are present. Twenty-four hypothetical leaky passive wells and one injection well are included in this analysis. The 25 wells are distributed over the nodes of a 5-rows by 5-columns regular grid. The spacing between extreme nodes along the coordinate directions (x and y) is 5 km. The injection well is positioned at the center node of this square grid. The distances between wells in the same row or in the same column are of 1 km. Three main scenarios with different CO₂ mass injection rates Q_m and durations are simulated. Table 3 summarizes these scenarios. Note that the final injected mass of CO₂ is the same in all scenarios and equal to about 63 Mt.

Table 3. CO₂ injection rates and duration of injection of the multiphase flow simulations of the hypothetical system representative of the Michigan Basin.

[Table 3 here]

Fluid overpressure values Δp_{iw} nearby the injection well at final time t_{end} (Equation 10) resulting from multiphase flow simulations for the three scenarios of Table 3 are reported in Figure 5. Scenario S1 produces the greatest overpressure around the injection well with a value of 78 bar (1 bar $\equiv 1 \times 10^5$ Pa) at $t_{end} = 20$ years. On the other hand, scenario S3 produces the lowest overpressure nearby the injection well with a value of 33 bar at $t_{end} = 60$ years. Scenario S2 produces intermediate results between S1 and S3, with a $\Delta p_{iw} = 46$ bar at $t_{end} = 40$ years.

In Figure 5, the vertical dashed line represents the maximum admissible overpressure, Δp_{max} , that is, the overpressure threshold beyond which the caprock is likely to fissure. This threshold value is calculated as (Teatini et al., 2010):

$$\Delta p_{max} = \frac{\nu}{1-\nu} \sigma'_z \quad (20)$$

where: ν is the Poisson ratio and σ'_z is the estimated effective vertical stress at the caprock depth under pressostatic undisturbed conditions. Assuming a Poisson ratio of $\nu=0.25$, Δp_{max} is estimated to be equal to 72 bar. The results in Figure 5 show that the maximum overpressure allowed is exceeded only in Scenario S1. In practice, these results indicate that for a prescribed CO₂ mass injection target, lower injection rates over longer injection periods represent - in terms of caprock fracturing risk - a safer storage strategy than higher injection rates over shorter injection periods. Therefore S2 and S3 would be the safest for the GCS system not to fissure the sealing formation.

[Figure 5 here]

Figure 5. Fluid overpressure results nearby the injection well from the multiphase flow simulations of the hypothetical system based on the Michigan Basin for scenarios S1, S2, and S3 (Table 3). The vertical dashed line represents the maximum overpressure allowed at the injected formation.

Figure 6 shows results concerning the amount of CO₂ mass leaked into the overlying formations (L2, L3, and L4) estimated by multiphase flow simulation of the considered hypothetical system. This figure presents the % M_{leak} that escapes from the injected formation L1 and is stored into the overlying formations, L2, L3, and L4. Scenario S1 produces the lowest total percentage of CO₂ leaked from the injection formation with % $M_{leak}=0.014\%$ at $t_{end}=20$ years, while S3 produces the highest leakage with % $M_{leak}=0.020\%$ at $t_{end}=60$ years. Although scenario S1 produces the highest fluid overpressure nearby the injection well (Figure 5), it has the lowest CO₂ leakage. It is, however, important to observe that the resulting values of % M_{leak} for the three scenarios are generally small. From Figure 6, it can also be noticed that in all scenarios S1, S2, and S3, most of the leaked CO₂ tends to be stored in the lower aquifer L2.

[Figure 6 here]

Figure 6. Percent of CO₂ mass leaked to overlying formations (L2, L3, and L4) from the multiphase flow simulations of the hypothetical system based on the Michigan Basin for scenarios S1, S2, and S3 (Table 3).

The fact that scenario S3 produces greater leakage than scenario S1 can be explained by observing that the CO₂ leakage mass depends directly on the product between: (a) the “exposure time”, during which the carbon plume is in contact with the passive wells; and (b) the pressure gradients across these passive wells (Equations 9 and 11). Numerical tests (not shown in this study) indicate that for lower injection rates (*i.e.* scenario S3) the pressure gradients are generally smaller, while the exposure time is significantly longer, so that their overall product is larger than in the case of higher injection rates (e.g. scenario S1). However, a more consistent comparison for scenarios S1 and S3 would have been a comparison that considers the CO₂ leakage at the same t_{end} (e.g. 60 years), where t_{end} also includes a post-injection phase in scenario S1. Scenario S1 would have been composed by 20 years of injection followed by 40 years of post-injection and thus scenario S1 would have included the mass leakage that might occur during the post-injection. This could likely have led to a higher $\%M_{leak}$ for scenario S1 than scenario S3. Due to the restrictions of the multiphase-flow used here (see Section 2), this comparison cannot be carried out.

In summary, these tests show that scenario S3 produces significantly lower fluid overpressure nearby the injection well than the other two scenarios. At the same time, the differences in $\%M_{leak}$ over all scenarios at the end of the injection time may be considered negligible. Therefore, scenario S3 is the only one investigated in the following analyses.

5.2.2 Stochastic Analysis Results

In this section, we present results obtained from the SA. We study the effects of uncertainty on injection aquifer permeability k_1 , injection aquifer φ_1 , passive well permeability k_{pw} , system

compressibility c_{eff} , brine residual saturation s_b^{res} and the CO₂ end-point relative permeability k_{r,CO_2} on the two state variables of interest: Δp_{iw} (Equation 10) and $\%M_{leak}$ (Equation 12).

Results from stochastic flow simulations are used to derive CDFs (see Section 3) for these state variables. These CDFs may be used to estimate the probability of fracturing the caprock, and the probability of CO₂ mass leakage not to exceed given threshold values. To analyze the risk of fracturing the caprock formations we consider “safe” conditions when the 95th percentile of Δp_{iw} is below Δp_{max} as estimated by Equation (20). To investigate the risk of CO₂ mass leakage, we consider “safe” conditions when the 95th percentile of $\%M_{leak}$ does not exceed limits derived from maximum CO₂ leakage rates of 1% per one year as suggested by Pacala (2003). It is important to emphasize that this estimate is rather conservative since the limit proposed by Pacala (2003) represents CO₂ leakage rates back to the atmosphere, whereas we consider the mass of CO₂ that escapes the target storage formation as leaked and do not account for the processes of storage and attenuation that CO₂ may undergo within the overburden formations.

Effect of aquifer permeability. The permeability of the aquifer is expected to have a significant influence on the fluid overpressure, with low permeability values producing large overpressure. SA results for aquifer permeability as the uncertain input parameter are shown in Figure 7. Figure 7a shows the CDF of Δp_{iw} obtained by sampling the aquifer permeability from the PDF described in Table 2. Aquifer permeability uncertainty affects significantly the spread of the CDF. Its range varies between 1 bar and 450 bar (more than two orders of magnitude). This agrees with Mathias et al. (2013), who showed that the variability of formation injectivity was quite high in open aquifers. Figure 7b shows the CDF of $\%M_{leak}$ obtained by assuming uncertain aquifer permeability (Table 2). This figure shows that uncertainty on k_1 has also a significant influence on CO₂ leakage, with a CDF whose spread spans over more than two orders of magnitude, from a minimum value of 0.02% to a maximum value of 0.72%.

[Figure 7 here]

Figure 7. CDF of the (a) fluid overpressure nearby the injection well, and (b) %CO₂ mass leakage associated with the uncertainty on aquifer permeability.

Figure 8 shows the percent of CO₂ mass leaked as a function of aquifer permeability. In general, lower permeability values correspond to increased mass leakage since higher fluid overpressures are obtained, which drive higher CO₂ flow rates through passive wells. On the contrary, the CO₂ plume advances faster through injection formations with higher permeabilities, increasing CO₂ storage in the injection aquifer.

[Figure 8 here]

Figure 8. %CO₂ mass leakage as a function of aquifer permeability.

Effect of aquifer porosity. SA results for uncertain aquifer porosity (Table 3) are presented in Figure 9a for Δp_{iw} and Figure 9b for % M_{leak} , respectively. The CDF in Figure 9a shows that uncertainty on formation porosity has a weak impact on the statistical variability of the maximum fluid overpressure at the injection well. Figure 9a reveals that Δp_{iw} varies between approximately 30 and 41 bars, resulting in a very small spread of the CDF. In general, larger porosities produce larger values of overpressure. Propagation of the overpressure pulse depends on porosity (Equation 2), in such a way that the same amount of CO₂ occupies a smaller region of the aquifer, hence retarding the attenuation of the overpressure pulse.

[Figure 9 here]

Figure 9. CDF of the (a) fluid overpressure nearby the injection well, and (b) %CO₂ mass leakage associated with the uncertainty on aquifer porosity.

Uncertainty on formation porosity has also a minor effect on the variability of CO₂ mass leakage. Smaller porosities are generally expected to result in larger leakage rates. Indeed, the shape of the plume depends on porosity (Equation 6) and lower porosities result in faster plume propagation and a higher likelihood of encountering leakage pathways. However, Figure 9b shows that the variability of CO₂ mass leakage is relatively contained since the CDF spread is less than one order of magnitude. Comparison of Figure 7 and Figure 9 indicates that uncertainty on porosity φ_1 has a much lower influence on fluid overpressure and CO₂ mass leakage than the uncertainty on injected formation permeability k_1 .

Effect of passive well permeability. Stochastic simulation results indicate that the fluid overpressure nearby the injection well is rather insensitive to passive well permeabilities k_{pw} . The CDF of Δp_{iw} is consequently not presented here. This result can be easily explained by noting that, for the geological setting investigated here (Section 5.1), fluid overpressure depends upon “local” conditions around the injection well, such as injection rate and formation permeability, rather than on conditions in regions of the domain “away” from the well.

On the other hand, the SA shows that uncertainty on leakage passive well permeability has a strong impact on CO₂ mass leakage. Figure 10 displays the CDFs of $\%M_{leak}$ corresponding to the three PDFs for the passive well permeability k_{pw} given in Table 2.

[Figure 10 here]

Figure 10. CDF of %CO₂ mass leakage associated with the uncertainty on passive well permeability. See Table 2 for descriptions of Case 1 – Case 3.

Although the three PDFs have the same median value of k_{pw} , the CDFs for CO₂ mass leakage are substantially different. In Figure 10 one may observe that in Case 1 (Table 2, lognormal PDF) the probability of CO₂ leakage is typically the smallest except for values of k_{pw} sampled from the upper tail of its distribution. Case 1 also presents the largest CDF spread (more than one order of magnitude),

whereas in Cases 2 and 3 the spread of the CDF is hardly noticeable. In Cases 2 and 3, k_{pw} is sampled from binary distributions (Table 2) characterized by two equally likely values, $1 \times 10^{-17} \text{ m}^2$ and $1 \times 10^{-11} \text{ m}^2$ in Case 2, and $1 \times 10^{-16} \text{ m}^2$ and $1 \times 10^{-12} \text{ m}^2$ in Case 3. Figure 10 shows that CO₂ mass leakage is probabilistically larger in Case 2, which indicates that the intensity of leakage is largely affected by the presence of highly permeable passive wells. Influence of the assignment of permeability at the passive wells on the amount of CO₂ leakage was identified in Celia et al. (2011).

Effect of system compressibility. The system compressibility is expected to have an impact on the fluid overpressure and mass leakage, with low values of c_{eff} producing greater values of fluid overpressure Δp_{iw} , and consequently higher $\%M_{leak}$. SA results under uncertain c_{eff} (Table 2) are presented in Figure 11. Figure 11a shows the CDF of Δp_{iw} , which varies between 1 and 68 bar.

The CDF of $\%M_{leak}$ shown in Figure 11b, indicates that system the compressibility has a significant impact on the variability of CO₂ mass leakage (about two orders of magnitude). However, the comparison of Figure 7b and Figure 11b reveals that the spread of the CDF is smaller than that obtained with uncertain aquifer permeability.

[Figure 11 here]

Figure 11. CDF of the (a) fluid overpressure nearby the injection well, and (b) %CO₂ mass leakage associated with the uncertainty on system compressibility.

Figure 12 shows fluid overpressure and percent of CO₂ mass leakage as functions of system compressibility, suggesting that lower values of system compressibility lead to larger fluid overpressure and larger leakage. In general, larger values of c_{eff} results in lower values of Δp_{iw} since the propagation of the pressure pulse depends on system compressibility (Equations 2 and 5), and the outer boundary of the pressure pulse will be smaller (Equation 5). Hence, a smaller region of the aquifer accepts the same amount of CO₂ given the larger storage capacity deriving from the deformability of the porous medium.

[Figure 12 here]

Figure 12. Fluid overpressure (left vertical axis) and %CO₂ mass leakage (right vertical axis) as functions of system compressibility.

Effect of brine residual saturation. SA results for uncertain brine residual saturation are presented in Figure 13a for Δp_{iw} and Figure 13b for % M_{leak} , respectively. In these tests, both s_b^{res} and $k_{r,c0}$ constitute uncertain variables, which are linked together by the relationship of statistical correlation derived in Section 5.1 (Figure 3). According to this correlation, as the brine residual saturation increases the $k_{r,c0}$ decreases. The CDF in Figure 13a shows that uncertainty from brine residual saturation s_b^{res} has an effect on the Δp_{iw} , which varies between 35 and 146 bar. This is in agreement with Celia et al. (2011), in which the maximum injection rate is limited to the maximum pressure allowed in the aquifer and it decreases when s_b^{res} is greater. However, the spread of the CDF is less than one order of magnitude. Figure 13b exposes that the impact of s_b^{res} on % M_{leak} is less important. The spread of its CDF is contained in half order of magnitude. In general, greater s_b^{res} values result in greater fluid overpressures and slightly larger leakage rates. Certainly, the extension of the CO₂ plume depends on brine residual saturation and greater values of s_b^{res} result in a more pronounced plume propagation and a higher likelihood of encountering leakage pathways Celia et al. (2011).

[Figure 13 here]

Figure 13. CDF of the (a) fluid overpressure nearby the injection well, and (b) %CO₂ mass leakage associated with the uncertainty on brine residual saturation.

If uncertainty of brine residual saturation is increased to 0.85 (maximum s_b^{res} value in Figure 3), so that its uniform PDF varies between 0 and 0.85, the effect of s_b^{res} on Δp_{iw} is increased. CDF of Δp_{iw} spreads from 35 to 235 bar. When increasing s_b^{res} , the effective porosity available to store CO₂ is reduced, which results in an increment of the fluid overpressure of the injection formation. If uncertainty on s_b^{res} is increased, then % M_{leak} increases, however the impact on its CDF is less noticeable.

Figure 14 shows the fluid overpressure and percent of CO₂ mass leaked as a function of $k_{r,c0}$. Lower values of $k_{r,c0}$ corresponds to higher values of Δp_{iw} and % M_{leak} . However, uncertainty of Δp_{iw} and % M_{leak} caused by s_b^{res} (and consequently also by $k_{r,c0}$) is less significant than uncertainty caused, for example, by k_1 or c_{eff} . The tendency of the fluid pressure to increase for lower $k_{r,c0}$ values and the fact that its impact is less important than the produced by injection formation permeability is in agreement with the observations of Mathias et al. (2013).

[Figure 14 here]

Figure 14. (a) Fluid overpressure nearby the injection well, and (b) %CO₂ mass leakage as a function of CO₂ end-point relative permeability.

General considerations from the SA applied to the Michigan Basin test site. In order to make general considerations on the feasibility of GCS for the Michigan Basin test site, a SA under Scenario S3 is carried out considering all parameters of Table 2 uncertain at the same time. For passive well permeability, the PDF of Case 1 (Table 2) is considered since is the situation that produces the greatest CDF spread as well as the largest values of % M_{leak} . The CDFs of Δp_{iw} and % M_{leak} calculated from this SA are given in Figure 15.

[Figure 15 here]

Figure 15. CDF of the (a) fluid overpressure nearby the injection well, and (b) %CO₂ mass leakage associated with the uncertainty on all uncertain parameters for scenarios S3 and S4. The vertical dashed line in (a) represents the maximum overpressure allowed at the injected formation and in (b) the %CO₂ mass leakage threshold.

The solid black line in Figure 15a represents the CDF of Δp_{iw} under Scenario S3. In the same graph, the vertical dashed line represents the maximum fluid overpressure $\Delta p_{max}=72$ bar allowed in the formation to avoid fracturing of the caprock (Equation 20). The intersection of this vertical line with the CDF of Δp_{iw} shows that in scenario S3 there is a 65% probability of not exceeding Δp_{max} . Likewise, the solid black line in Figure 15b represents the CDF of % M_{leak} under Scenario S3. The 1% CO₂ mass leakage threshold defined by Pacala (2003) is represented by the vertical dashed line. Based on the CDF of % M_{leak} , there appears to be a 87% probability of not exceeding such threshold.

In order to increase both the 65% probability of not fissuring the caprock and the 87% probability of not exceeding the 1% CO₂ mass leakage threshold to 95%, a new injection scenario S4 is investigated. In this scenario, the total amount of injected CO₂ is reduced by 76%, with an injection rate $Q_m = 8$ kg/s and an injection period $t_{end} = 50$ years. The SA for Scenario S4 leads to the CDFs of Δp_{iw} and % M_{leak} represented by the dotted profiles in Figure 15a and Figure 15b, respectively. Under this new scenario, the probabilities of not exceeding both $\Delta p_{max} = 72$ bar and % $M_{leak} = 1\%$ are increased to 95%.

The need to reduce the total mass injected from Scenario S3 to S4 in order to meet the prescribed safety constraints on Δp_{iw} and % M_{leak} is due to a “conflict” existing between these constraints when injecting a given mass of CO₂ ($\rho_c Q_m t_{end}$). Indeed, increasing the CO₂ injection rate Q_m and decreasing the injection time t_{end} is beneficial towards reducing % M_{leak} , but also increases the probability that Δp_{iw} exceeds Δp_{max} . Vice versa, decreasing Q_m and increasing t_{end} reduces the probability of fracturing the caprock, but increases the probability of violating the 1% threshold for % M_{leak} . Therefore, in order to comply with the requirement of both safety constraints, $\Delta p_{max} = 72$ bar and % $M_{leak} = 1\%$, the total mass

of injected CO₂ must be necessarily reduced by adequately decreasing both the injection rate Q_m and the injection time t_{end} .

5.2.3 Results of Global Sensitivity Analysis

In this section, we present results of the application of the extended FAST methodology to the Michigan Basin deep saline aquifer. The sensitivities of the 24 uncertain parameters (aquifer permeability, aquifer porosity, permeability of 20 potential passive well pathways, system compressibility, and brine residual saturation) on the variability of the outputs Δp_{iw} (Equation 10) and $\%M_{leak}$ (Equation 12) are studied. For the permeability of passive wells, the PDF of Case 1 (Table 2) is chosen since, in the SA, this has been shown to produce the largest spread of the $\%M_{leak}$ CDF (see Section 5.2.2).

The GSA results are presented in Figure 16 and in Table 4. Figure 16 shows pie charts for Δp_{iw} and $\%M_{leak}$, where each total effect index S_{T_i} (Equation 15) is represented by the “normalized” percentage:

$$\%S_{T_i} = \frac{S_{T_i}}{\sum_{i=1}^n S_{T_i}} 100 \quad (21)$$

where n is the total number of uncertain input parameters, in this case equal to 24. In this figure, the combined effect of the 20 leakage pathways is grouped and denoted as k_{pw1-20} . Table 4 displays the first-order sensitivity indices S_i as a percentage of the total effect indices S_{T_i} for both Δp_{iw} and $\%M_{leak}$.

[Figure 16 here]

Figure 16. Extended FAST normalized total effect indices for: (a) maximum fluid overpressure in the vicinity of the injection well, and (b) %CO₂ mass leakage.

Table 4. Extended FAST First-order effects as a percentage of the total effect for fluid overpressure at the vicinity of the injection well, and %CO₂ mass leakage.

[Table 4 here]

Fluid overpressure nearby the injection well. Figure 16a illustrates the normalized total effect indices $\%S_{T_i}$ for the fluid overpressure nearby the injection well. The variability of Δp_{iw} is mainly influenced by only two parameters, that is, the aquifer permeability k_1 and the compound effect of passive well permeabilities k_{pw1-20} , which altogether account for about 73% of the overall Δp_{iw} variance. Of this 73%, 42% is due to k_1 and 31% is due to k_{pw1-20} . However, the maximum total effect of one individual passive well permeability is only 3%. The prominent influence of k_1 is somehow expected since the propagation of the pressure pulse is mainly governed by the aquifer permeability (Equations 2 and 5). When k_1 has a large value, the overpressure pulse can propagate easily through the injected formation moving away from the injection well and producing lower Δp_{iw} values and vice versa. Residual saturation accounts for 18% of the total variance ($\%S_{T_{s_b^{res}}} = 18\%$). When s_b^{res} increases, both the end-point relative permeability $k_{r,c0}$ (Figure 3) and the effective volume of porosity available to store CO_2 decrease, resulting in an increment of the fluid overpressure. Figure 16a indicates that the porosity and system compressibility have small impacts on the variability of Δp_{iw} , with a $\%S_T$ equal to 4% and 5% respectively. These results indicate that the total effect indices of porosity, system compressibility, and pathway permeability are negligible, so that their uncertainty has a limited impact on the variability of the fluid overpressure nearby the injection well.

In Table 4 one may observe that only aquifer permeability k_1 affects the variability of Δp_{iw} mostly through the first-order index with $S_{k_1} = 63.1\%$ of the total effect index. The contribution of brine residual saturation s_b^{res} to the variability of Δp_{iw} derives from the interaction with other parameters ($S_{s_b^{res}} = 30.0\% < S_{I_{s_b^{res}}} = 70.0\%$). The contribution of porosity φ_1 , system compressibility c_{eff} , and passive well permeabilities k_{pw_i} ($i=1,2,\dots,20$) is less than 3.5% from the first-order effect, most of their effects come from higher-order effects (>97%) or interaction with other parameters.

CO₂ mass leakage. Figure 16b illustrates results of total effect index normalized on $\%M_{leak}$ variance. This figure shows that the spread of the CO₂ mass leakage output is mainly influenced by the passive well permeability as a group with $\%S_{T_{k_{pw1-20}}} = 66\%$. However, the maximum total effect index coming from an individual pathway permeability cluster is 8%. The total effect index normalized of the aquifer permeability is $\%S_{T_{k_1}} = 12\%$, followed by the aquifer porosity with $\%S_{T_{\phi_1}} = 10\%$, and system compressibility with $\%S_{T_{c_{eff}}} = 9\%$. Therefore, the aquifer permeability has a larger total effect index than the pathway permeability of any of the 20 clusters has. The brine residual saturation contributes to the $\%M_{leak}$ variability for about 4%. The contribution of s_b^{res} (and $k_{r,c0}$) to the $\%M_{leak}$ variability is lower than the contribution to the Δp_{iw} variability. The total effect index for s_b^{res} can be considered negligible. In other words, any value of s_b^{res} selected from the PDF presented in Table 2 seems to produce a small variability of CO₂ mass leakage.

Table 4 lists the first-order sensitivity index for each of the 24 uncertain parameters as a percentage of the total effect on $\%CO_2$ mass leakage. One can observe that the main contribution to the $\%M_{leak}$ variability comes from higher-order effects. Aquifer permeability, aquifer porosity and system compressibility have the largest contribution from the first-order index with a value of about 20%. Pathway permeability of clusters 6, 11 and 16 also present a large contribution from the first-order index in comparison to the other pathways. The leakage pathway permeability that presents the greatest contribution from the first-order sensitivity index is k_{pw_16} with a value of 24%. Indeed this is the passive well cluster closest to the injection well, which shows that the location of leakage pathways is an important component on the contribution to $\%M_{leak}$ variability. Higher-order effects from all uncertain parameters have a larger impact on the variability of $\%M_{leak}$ than their respective first-order effects.

General considerations from the GSA applied to the Michigan Basin test site. GSA results for fluid overpressure confirm some of the observations already made in the SA and also provide new insights. A large portion of the Δp_{iw} variability is attributed to only two parameters: aquifer permeability and brine residual saturation. Notice that in the SA, aquifer permeability, brine residual saturation

together with system compressibility are the most uncertain parameters of the Δp_{iw} . By far, aquifer permeability is the most influential parameter as it ranks in first position with a normalized S_T equal to 42%. In order to significantly reduce the prediction of Δp_{iw} , acquiring accurate data of aquifer permeability is of primary importance.

From the GSA results for $\%M_{leak}$, one can conclude that aquifer permeability, aquifer porosity, system compressibility, and pathway permeability have the most significant impact on the variability of the output. Brine residual saturation also shows an impact, although this is minor in comparison to the other parameters. Location of leakage pathways closer to the injection well shows a significant effect on $\%M_{leak}$ with significantly higher first-order indices respect to passive wells located farther away. Therefore, when interested in studying uncertainty and risk of CO₂ leakage, an effort to acquire data concerning aquifer permeability, aquifer porosity, system compressibility, and location and permeability of potential leakage pathways is essential to reduce the uncertainty in the simulation of $\%M_{leak}$.

6 Summary and Conclusions

In this work, we have analyzed the variability of fluid overpressure in proximity of injection wells and CO₂ mass leakage of a candidate site for GCS located within the Michigan Basin. This study relied on a stochastic analysis and a global sensitivity analysis accounting for the uncertainty on the following: permeability and porosity of injection formation, permeability of passive wells, system compressibility, brine residual saturation and the CO₂ end-point relative permeability. From the investigation of potential injection scenarios, it was observed that lower injection rates with longer injection times reduce the probability of producing excessive fluid overpressures in the injection aquifer. As far as CO₂ mass leakage is concerned, there was a small difference among these scenarios. Therefore, injection of CO₂ at low rates and protracted for a longer period of time appears to be the most convenient policy for the safety of the GCS system.

The stochastic analysis showed that the most influential parameter on both fluid overpressure and CO₂ mass leakage is the aquifer permeability. Fluid overpressure in proximity of injection well was also affected by system compressibility and brine residual saturation, and it seems unaffected by uncertainty on porosity. On the other hand, CO₂ mass leakage is shown to be particularly sensitive to passive well permeability and the type of statistical distribution used to characterize uncertainty in it. CO₂ mass leakage is also affected by the system compressibility. The stochastic analysis also revealed that constraints on maximum overpressure and maximum leakage are competing against one another when injecting the same mass of CO₂. This resulted in a reduction of the CO₂ injection rate and injection time, so that 95% of the cases do not exceed both maximum thresholds of fluid overpressure and CO₂ mass leakage.

Results from the extended FAST global sensitivity analysis confirmed some of the outcomes of the stochastic analysis, however providing more detail. Injection formation permeability and brine residual saturation combined with CO₂ end-point relative permeability had the greatest impact on fluid overpressure. The influence of the injection formation permeability on pressure buildup is due mostly by first-order effect and about one third is due to its interaction with the other parameters. On the other hand, the impact of brine residual saturation and CO₂ end-point relative permeability on pressure buildup variance is mostly due to their interaction with other parameters (higher order effects). CO₂ mass leakage is mainly influenced by passive well permeability and aquifer permeability, followed by the aquifer porosity and system compressibility. The influence of these parameters on CO₂ mass leakage is mainly produced by higher order effects. The important interaction of higher order effects of these parameters on the CO₂ mass leakage has been revealed by the GSA. When studying the variability on the fluid overpressure, individual permeability of the leakage pathways, aquifer porosity and system compressibility resulted to have a low impact. On the other hand, the effect of leakage pathways with respect to the variability on CO₂ mass leakage is significant and cannot be neglected, especially for passive wells located closer to the injection well. This analysis also showed that influence of passive well permeability on CO₂ mass leakage mostly is produced by the interaction of passive well permeability with

other parameters. Interestingly, the GSA provided more information about the system compressibility parameter. It showed that its influence on the outputs is not as important as the SA indicated.

From these analyses, we can conclude that efforts to obtain further information about influent parameters, such injection formation permeability is necessary when studying their impact on fluid overpressure and CO₂ mass leakage for the Michigan Basin test site. In addition, recollection of leakage pathway information, especially from pathways located closer to the injection well is needed for quantifying potential CO₂ mass leakages with higher degree of confidence. Additionally, this study aims at being a role model to be followed when considering the selection and appropriateness of other potential GCS candidate sites. The approach to sensitivity analysis founded on SA and GSA is based on solid statistical tools that can highlight and quantify aspects of uncertainty in unique ways; thus similar methodologies should be followed to study GCS feasibility at other sites. However, one should bear in mind that formation parameters and the position and quantity of passive wells to analyze will vary from site to site. SA can provide information about the output spread, which is an indicator of the parameter's impact on the output. Also, SA can provide information about the probability of exceeding predefined threshold values, such as the maximum fluid overpressure allowed at the caprock formation and the maximum amount of leaked CO₂ to overlying aquifers. The large numbers of parameters required by modeling CO₂ injection into a deep saline aquifer are often difficult to obtain and consequently present large uncertainties. GSA can separate the most significant input parameters from the less important and assess their relative contributions to the overall output uncertainty. This can be extremely helpful to allocate resources effectively.

Acknowledgements

This research was supported by the U. S. Department of Energy, National Energy Technology Laboratory (DOE Project: DE-FE0001830). The global sensitivity analysis of extended FAST was carried out with SimLab, a free development framework for Sensitivity and Uncertainty Analysis (<http://ipsc.jrc.ec.europa.eu/?id=756>).

7 References

- Aoyagi, R., Kitamura, O., Itaoka, K., Igawa, S., Suzuki, S., 2011. Study on role of simulation of possible leakage from geological CO₂ storage in sub-seabed for environmental impact assessment. *Energy Procedia* 4, 3881-3888.
- Aschenbrenner, B.C., Chilingar, G.V., 1960. Teodorovich's Method for Determining Permeability from Pore-Space Characteristics of Carbonate Rocks: GEOLOGICAL NOTES. *AAPG Bulletin* 44, 1421-1424.
- Bachu, S., 2003. Screening and ranking of sedimentary basins for sequestration of CO₂ in geological media in response to climate change. *Environmental Geology* 44, 277-289.
- Bennion, B., Bachu, S., 2008. Drainage and Imbibition Relative Permeability Relationships for Supercritical CO₂/Brine and H₂S/Brine Systems in Intergranular Sandstone Carbonate Shale and Anhydrite Rocks. *SPE Reservoir Evaluation & Engineering* 11, 487-496.
- Bennion, D., Bachu, S., 2010. Drainage and imbibition CO₂/brine relative permeability curves at reservoir conditions for carbonate formations, *SPE Annual Technical Conference and Exhibition*, p. 18.
- Bergman, P.D., Winter, E.M., 1995. Disposal of carbon-dioxide in aquifers in the US. *Energy Conversion and Management* 36, 523-526.
- Beven, K., 1993. Prophecy, reality and uncertainty in distributed hydrological modelling. *Adv Water Resour* 16, 41-51.
- Celia, M.A., Nordbotten, J.M., 2009. Practical Modeling Approaches for Geological Storage of Carbon Dioxide. *Ground Water* 47, 627-638.
- Celia, M.A., Nordbotten, J.M., Bachu, S., Dobossy, M., 2009. Risk of leakage versus depth of injection in geological storage. *Energy Procedia* 1, 2573-2580.
- Celia, M.A., Nordbotten, J.M., Court, B., Dobossy, M., Bachu, S., 2011. Field-scale application of a semi-analytical model for estimation of CO₂ and brine leakage along old wells. *International Journal of Greenhouse Gas Control* 5, 257-269.
- Cody, B., Baù, D., González-Nicolás, A., 2014. Improved Semi-Analytical Simulation of Geological Carbon Sequestration (in review). *Computational Geosciences*.
- Cukier, R., Levine, H., Shuler, K., 1978. Nonlinear sensitivity analysis of multiparameter model systems. *Journal of computational physics* 26, 1-42.
- Dentz, M., Tartakovsky, D.M., 2009. Abrupt-Interface Solution for Carbon Dioxide Injection into Porous Media. *Transport in Porous Media* 79, 15-27.
- Dobossy, M.E., Celia, M.A., Nordbotten, J.M., 2011. An efficient software framework for performing industrial risk assessment of leakage for geological storage of CO₂. *Energy Procedia* 4, 4207-4214.
- Gasda, S.E., Celia, M.A., Nordbotten, J.M., 2008. Upslope plume migration and implications for geological CO₂ sequestration in deep, saline aquifers. *The IES journal. Part A, Civil & structural engineering* 1, 15.
- Gupta, A.K., Bryant, S.L., 2011. Analytical Correlations for Risk Parameters Involved in CO₂ Storage. *Energy Procedia* 4, 3849-3856.
- Hahn, G.J., 1967. *Statistical models in engineering*. Wiley, New York.
- Halliburton, 1990. Log 21101375660000 Stech Upper Half (Date: 09/04/1990).
- International Energy Agency, 2008. *Carbon Capture and Storage: Meeting the Challenge of climate change*, Paris.
- Kano, Y., Ishido, T., 2011. Numerical simulation on the long-term behavior of CO₂ injected into a deep saline aquifer composed of alternating layers. *Energy Procedia* 4, 4339-4346.
- Kopp, A., Binning, P.J., Johannsen, K., Helmig, R., Class, H., 2010. A contribution to risk analysis for leakage through abandoned wells in geological CO₂ storage. *Adv Water Resour* 33, 867-879.
- Kutchko, B.G., Strazisar, B.R., Huerta, N., Lowry, G.V., Dzombak, D.A., Thaulow, N., 2009. CO₂ reaction with hydrated class H well cement under geologic sequestration conditions: effects of flyash admixtures. *Environ Sci Technol* 43, 3947-3952.

LeNeveu, D.M., 2008. CQUESTRA, a risk and performance assessment code for geological sequestration of carbon dioxide. *Energy Conversion and Management* 49, 32-46.

Li, H., Zhang, D., 2007. Probabilistic collocation method for flow in porous media: Comparisons with other stochastic methods. *Water Resour Res* 43.

Mathias, S.A., Gluyas, J.G., González Martínez de Miguel, G.J., Bryant, S.L., Wilson, D., 2013. On relative permeability data uncertainty and CO₂ injectivity estimation for brine aquifers. *International Journal of Greenhouse Gas Control* 12, 200-212.

Mathias, S.A., Gluyas, J.G., González Martínez de Miguel, G.J., Hosseini, S.A., 2011. Role of partial miscibility on pressure buildup due to constant rate injection of CO₂ into closed and open brine aquifers. *Water Resour Res* 47.

McIntyre, N., Jackson, B., Wade, A., Butterfield, D., Wheeler, H., 2005. Sensitivity analysis of a catchment-scale nitrogen model. *Journal of Hydrology* 315, 71-92.

MDEQOGD, 2014. Michigan Department of Environmental Quality Oil and Gas Database, http://www.michigan.gov/deq/0,4561,7-135-6132_6828-98518--,00.html. Accessed 03/08/2014.

Middleton, R.S., Keating, G.N., Viswanathan, H.S., Stauffer, P.H., Pawar, R.J., 2012. Effects of geologic reservoir uncertainty on CO₂ transport and storage infrastructure. *International Journal of Greenhouse Gas Control* 8, 132-142.

Morris, M.D., 1991. Factorial sampling plans for preliminary computational experiments. *Technometrics* 33, 161-174.

Nogues, J.P., Court, B., Dobossy, M., Nordbotten, J.M., Celia, M.A., 2012. A methodology to estimate maximum probable leakage along old wells in a geological sequestration operation. *International Journal of Greenhouse Gas Control* 7, 39-47.

Nordbotten, J.M., Celia, M.A., 2006. Similarity solutions for fluid injection into confined aquifers. *Journal of Fluid Mechanics* 561, 307-327.

Nordbotten, J.M., Celia, M.A., Bachu, S., 2005a. Injection and storage of CO₂ in deep saline aquifers: Analytical solution for CO₂ plume evolution during injection. *Transport in Porous Media* 58, 339-360.

Nordbotten, J.M., Celia, M.A., Bachu, S., Dahle, H.K., 2005b. Semianalytical solution for CO₂ leakage through an abandoned well. *Environ Sci Technol* 39, 602-611.

Nordbotten, J.M., Kavetski, D., Celia, M.A., Bachu, S., 2009. Model for CO₂ Leakage Including Multiple Geological Layers and Multiple Leaky Wells. *Environ Sci Technol* 43, 743-749.

Oladyshkin, S., Class, H., Helmig, R., Nowak, W., 2011. An integrative approach to robust design and probabilistic risk assessment for CO₂ storage in geological formations. *Computational Geosciences* 15, 565-577.

Oldenburg, C.M., Bryant, S.L., Nicot, J.P., 2009. Certification framework based on effective trapping for geologic carbon sequestration. *International Journal of Greenhouse Gas Control* 3, 444-457.

Pacala, S.W., 2003. Global Constraints on Reservoir Leakage, in: Gale, J., Kaya, Y. (Eds.), *Greenhouse Gas Control Technologies - 6th International Conference*. Pergamon, Oxford, pp. 267-272.

Ruether, J.A., 1998. FETC Programs for Reducing Greenhouse Gas Emissions, Other Information: PBD: Feb 1998, p. Medium: ED; Size: 20 p.; Other: FDE: PDF; PL:.

Saltelli, A., 2008. *Global sensitivity analysis the primer*. John Wiley, Chichester, England.

Saltelli, A., Tarantola, S., Chan, K.-S., 1999. A quantitative model-independent method for global sensitivity analysis of model output. *Technometrics* 41, 39-56.

Saripalli, P., McGrail, P., 2002. Semi-analytical approaches to modeling deep well injection of CO₂ for geological sequestration. *Energy Conversion and Management* 43, 185-198.

SCH, 1983. Log 21101365880000 Burch Main Suite (Date 06/19/1983).

SCH, 1991. Log 21101375660000 Stech Lower Half (Date: 06/29/1991).

SIMLAB, 2007. Ver 2.2, <http://ipsc.jrc.ec.europa.eu/?id=756>, European Commission, Joint Research Centre, Ver 2.2 ed.

Sobol', I.M., 2001. Global sensitivity indices for nonlinear mathematical models and their Monte Carlo estimates. *Mathematics and Computers in Simulation* 55, 271-280.

- Solomon, S., Intergovernmental Panel on Climate Change., Intergovernmental Panel on Climate Change. Working Group I., 2007. Climate change 2007 : the physical science basis : contribution of Working Group I to the Fourth Assessment Report of the Intergovernmental Panel on Climate Change. Cambridge University Press, Cambridge ; New York.
- Stauffer, P.H., Viswanathan, H.S., Pawar, R.J., Guthrie, G.D., 2008. A system model for geologic sequestration of carbon dioxide. *Environ Sci Technol* 43, 565-570.
- Takahashi, W., 2000. *Nonlinear Functional Analysis, Fixed point theory and its applications*, p. iv+ 276. Yokohama, Yokohama, Japan.
- Teatini, P., Ferronato, M., Gambolati, G., Baù, D., Putti, M., 2010. Anthropogenic Venice uplift by seawater pumping into a heterogeneous aquifer system. *Water Resour Res* 46, W11547.
- Trebin, F.A., 1945. Permeability to oil of sandstone reservoir.
- Turpening, R., Toksöz, M., Born, A., al., e., 1992. Reservoir Delineation Consortium Annual Report, Massachusetts Institute of Technology, Cambridge.
- Van Genuchten, M.T., 1980. A Closed-form Equation for Predicting the Hydraulic Conductivity of Unsaturated Soils1. *Soil Science Society of America Journal* 44, 892.
- Vilarrasa, V., Bolster, D., Dentz, M., Olivella, S., Carrera, J., 2010. Effects of CO₂ Compressibility on CO₂ Storage in Deep Saline Aquifers. *Transport in Porous Media* 85, 619-639.
- Wainwright, H.M., Finsterle, S., Zhou, Q., Birkholzer, J.T., 2013. Modeling the performance of large-scale CO₂ storage systems: A comparison of different sensitivity analysis methods. *International Journal of Greenhouse Gas Control* 17, 189-205.
- Walter, L., Oladyshkin, S., Class, H., Darcis, M., Helmig, R., 2011. A study on pressure evolution in a channel system during CO₂ injection. *Energy Procedia* 4, 3722-3729.
- Wiener, N., 1938. The Homogeneous Chaos. *American Journal of Mathematics* 60, 897-936.
- Zhao, H.J., Liao, X.W., Chen, Y.F., Zhao, X.L., 2010. Sensitivity analysis of CO₂ sequestration in saline aquifers. *Petroleum Science* 7, 372-378.
- Zhou, Q., Birkholzer, J.T., Mehnert, E., Lin, Y.-F., Zhang, K., 2009. Modeling Basin- and Plume-Scale Processes of CO₂ Storage for Full-Scale Deployment. *Ground Water* 48, 494-514.

Table 1. Hydro-geomechanical parameters of the reference case. Parameters of this table remain unchanged (deterministic) unless the parameter of interest is considered uncertain

Parameter	Symbol	Value	Units
Brine density	ρ_b	1,045	kg m ⁻³
CO ₂ density	ρ_c	575	kg m ⁻³
Brine viscosity	μ_b	4.5×10^{-4}	Pa s
CO ₂ viscosity	μ_c	4.6×10^{-5}	Pa s
System compressibility	c_{eff}	4.6×10^{-10}	Pa ⁻¹
Injection aquifer porosity	φ_1	0.084	/
Overlying aquifer porosity	φ_2	0.05	/
Brine residual saturation	s_b^{res}	0.3	/
End-point CO ₂ relative permeability	$k_{r,c0}$	0.42	/
Injection aquifer permeability	k_1	2.8×10^{-14}	m ²
Overlying aquifer permeability	k_2	9.6×10^{-15}	m ²
Passive wells permeability	k_{pw}	1.0×10^{-14}	m ²

Table 2. Probability distribution functions (PDFs) for uncertain parameters

Parameter (unit)	Distribution	Median value	Log standard deviation	Minimum value	Maximum value	Realizations
Aquifer permeability (m ²)	lognormal	2.8×10^{-14}	0.5	-	-	1,000
Aquifer porosity (/)	uniform	-	-	0.05	0.35	1,000
Passive well permeability (m ²)	<u>Case 1</u>	1.0×10^{-14}	1	-	-	1,000
	<u>Case 2</u>	1.0×10^{-14}	-	1.0×10^{-17} *	1.0×10^{-11} *	1,000
	<u>Case 3</u>	1.0×10^{-14}	-	1.0×10^{-16} *	1.0×10^{-12} *	1,000

System compressibility (Pa ⁻¹)	lognormal	1.0×10 ⁻⁹	1	-	-	1,000
Brine residual saturation (/)	uniform	-	-	0.00	0.6	1,000

*Single value with 50% of probability. Minimum value corresponds to a well-cemented well and maximum value corresponds to a poorly-cemented well.

Table 3. CO₂ injection rates and duration of injection of the multiphase flow simulations of the hypothetical system representative of the Michigan Basin.

Scenario	Q_m (kg/s)	t_{end} (years)
S1	100	20
S2	50	40
S3	33.33	60

Table 4. Extended FAST First-order effects as a percentage of the total effect for fluid overpressure at the vicinity of the injection well, and %CO₂ mass leakage.

Uncertain parameter	% S_i of S_{Ti} Δp_{iw}	% S_i of S_{Ti} % M_{leak}	Uncertain parameter	% S_i of S_{Ti} Δp_{iw}	% S_i of S_{Ti} % M_{leak}
k_l	63.1	22.4	k_{pw9}	0.4	4.9
φ_l	3.2	18.6	k_{pw10}	0.4	0.4
c_{eff}	28.0	21.8	k_{pw11}	0.1	17.9
s_b^{res} and $k_{r,c0}$	30.0	4.2	k_{pw12}	1.6	1.2
k_{pw1}	1.1	0.6	k_{pw13}	0.3	2.9
k_{pw2}	0.5	0.6	k_{pw14}	0.4	2.7

k_{pw3}	0.3	1.4	k_{pw15}	0.6	3.7
k_{pw4}	0.9	0.7	k_{pw16}	0.8	24.0
k_{pw5}	0.9	0.1	k_{pw17}	0.6	2.3
k_{pw6}	1.3	10.5	k_{pw18}	0.2	1.9
k_{pw7}	1.2	0.8	k_{pw19}	2.1	2.6
k_{pw8}	0.2	3.5	k_{pw20}	0.6	0.8

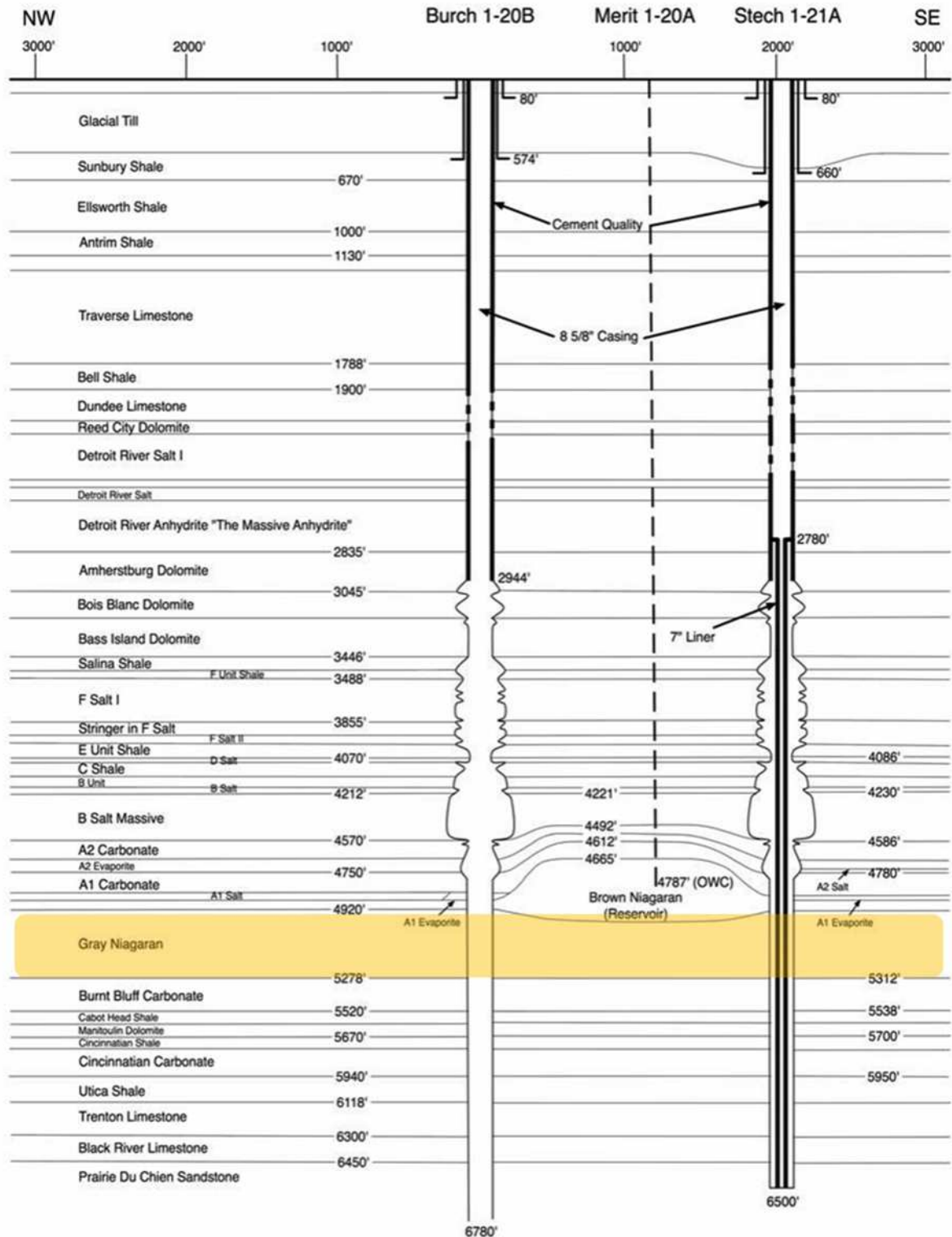


Figure 1. Cross-section of the Michigan Basin test site (adapted from (Turpening et al., 1992).

The Gray Niagaran formation highlighted in yellow, is selected as potential candidate for GCS.

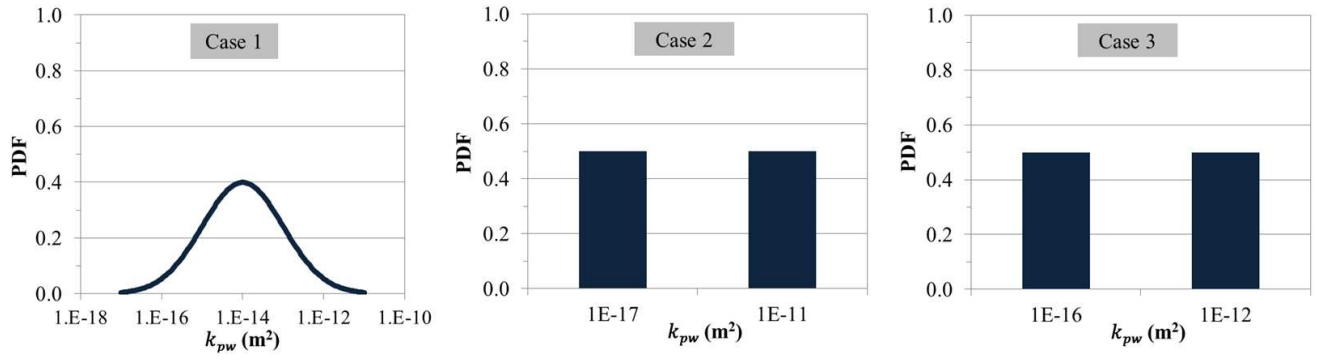


Figure 2. PDFs of passive well permeability assigned to Case 1, Case 2, and Case 3. Details of these PDFs are in Table 2.

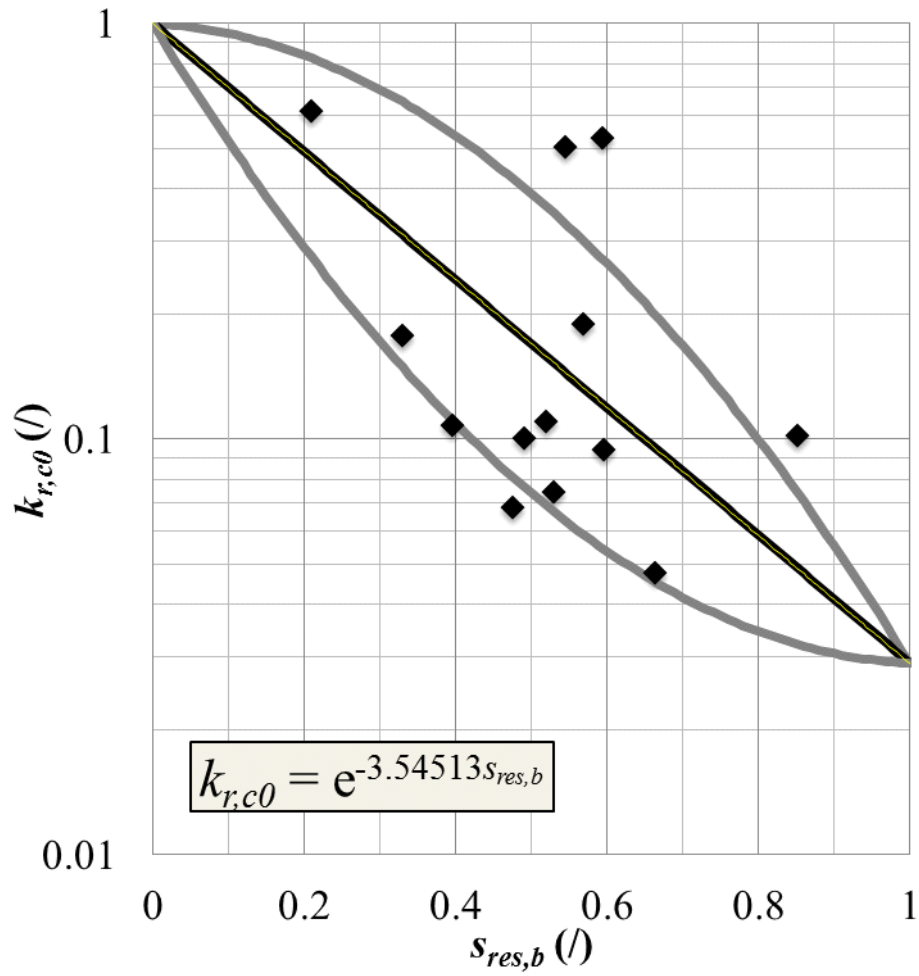


Figure 3. Representation of $k_{r,c0}$ and s_b^{res} data of carbonates/dolomites (Bennion and Bachu, 2008; Bennion and Bachu, 2010), exponential regression (in black), and the half amplitude of confidence interval (in grey).

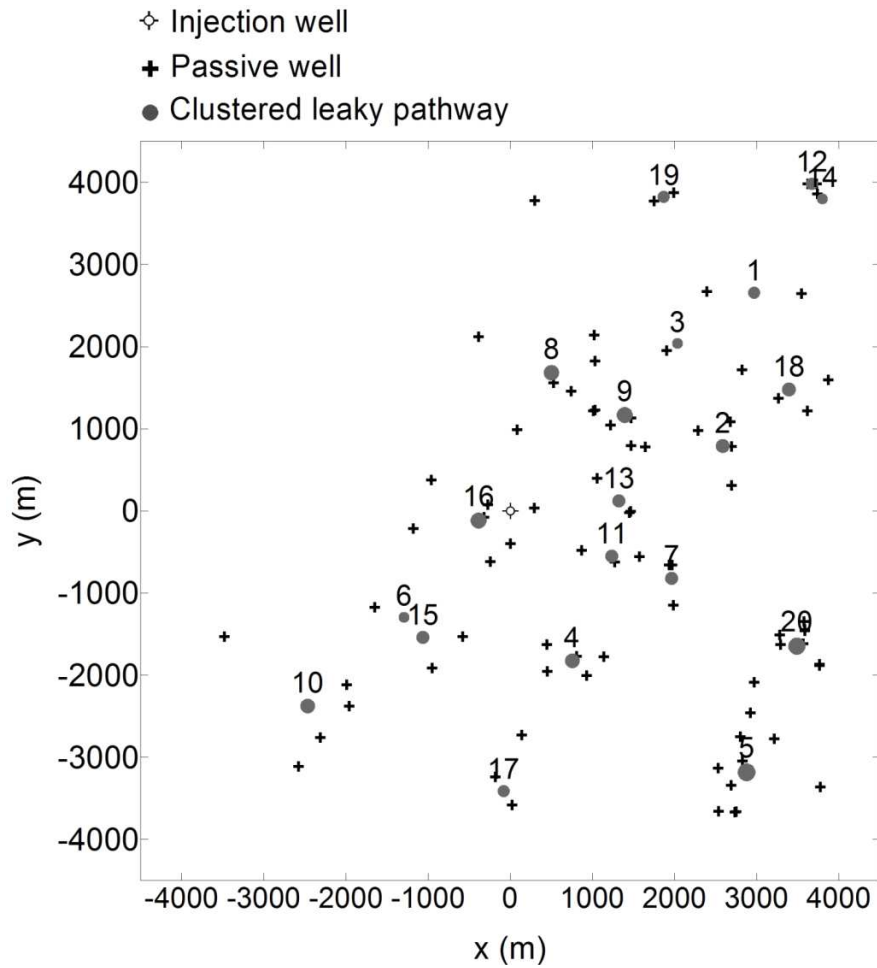


Figure 4. Location of the 80 passive wells (indicated as crosses) that reach the Niagaran formation and location of the 20 equivalent leakage pathways (indicated as circles) used in the GSA and obtained after clustering the 80 passive wells. The injection well is located at the center of the domain.

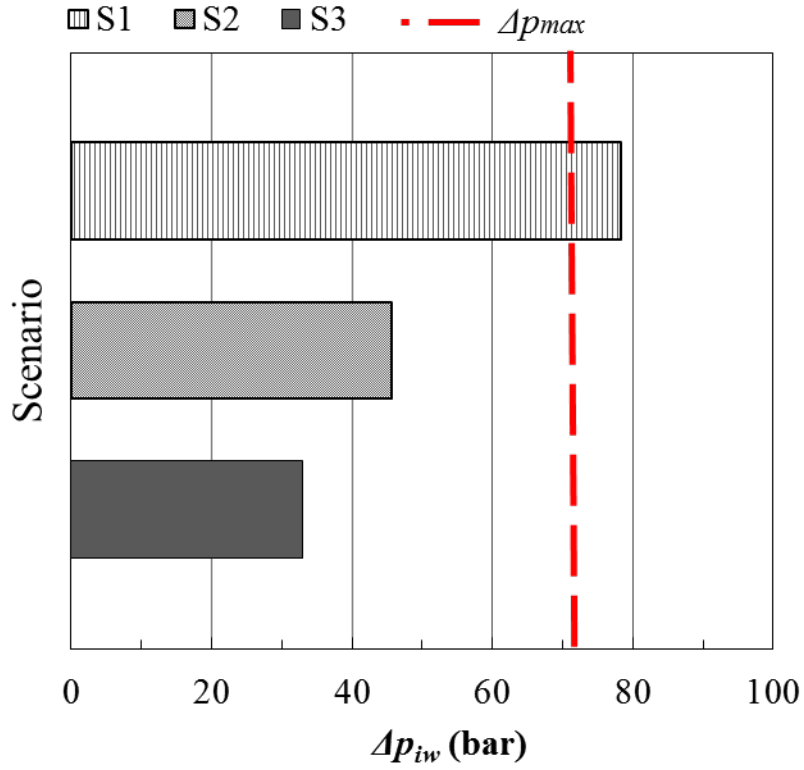


Figure 5. Fluid overpressure results nearby the injection well from the multiphase flow simulations of the hypothetical system based on the Michigan Basin for scenarios S1, S2, and S3 (Table 3). The vertical dashed line represents the maximum overpressure allowed at the injected formation.

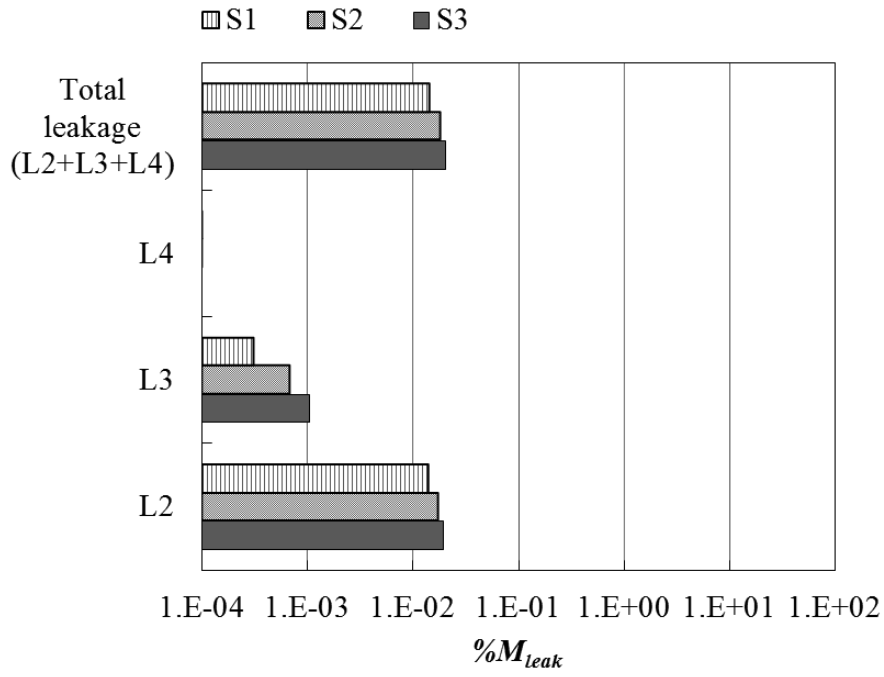


Figure 6. Percent of CO₂ mass leaked to overlying formations (L2, L3, and L4) from the multiphase flow simulations of the hypothetical system based on the Michigan Basin for scenarios S1, S2, and S3 (Table 3).

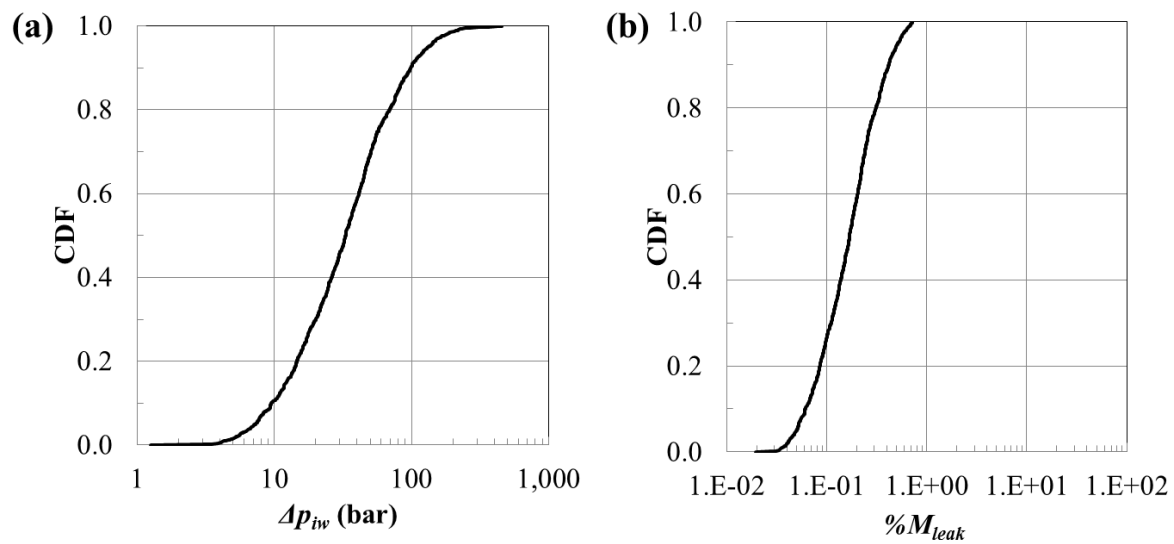


Figure 7. CDF of the (a) fluid overpressure nearby the injection well, and (b) %CO₂ mass leakage associated with the uncertainty on aquifer permeability.

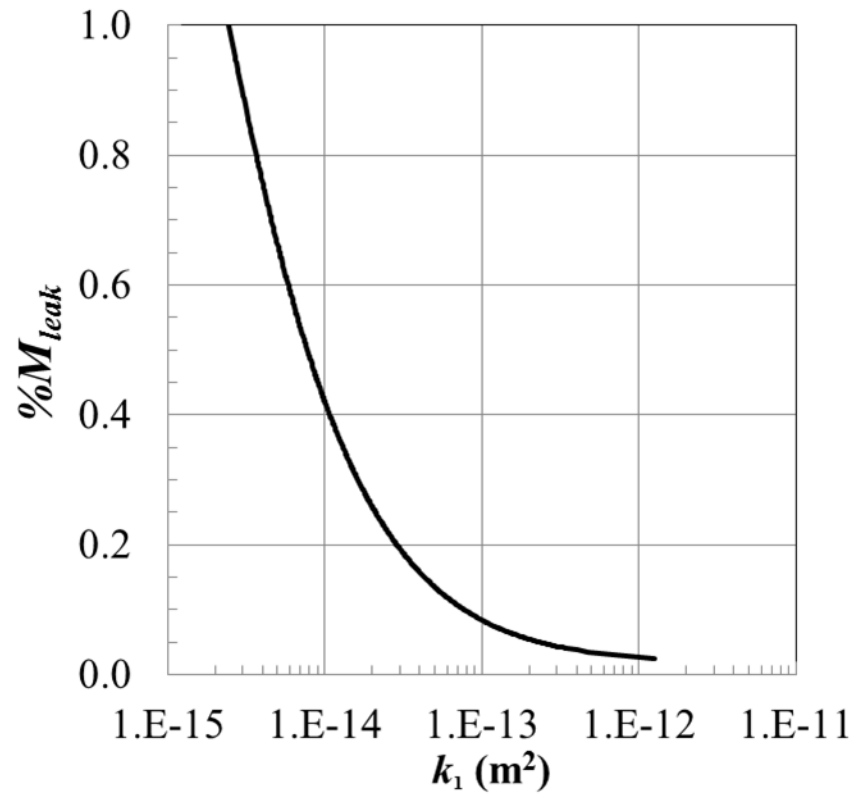


Figure 8. %CO₂ mass leakage as a function of aquifer permeability.

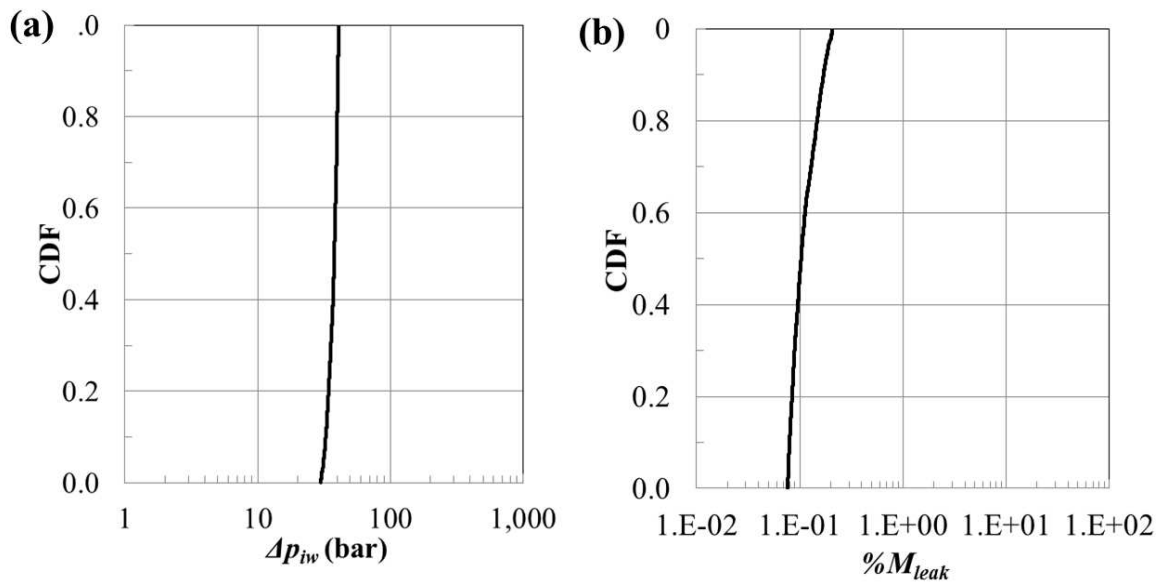


Figure 9. CDF of the (a) fluid overpressure nearby the injection well, and (b) %CO₂ mass leakage associated with the uncertainty on aquifer porosity.

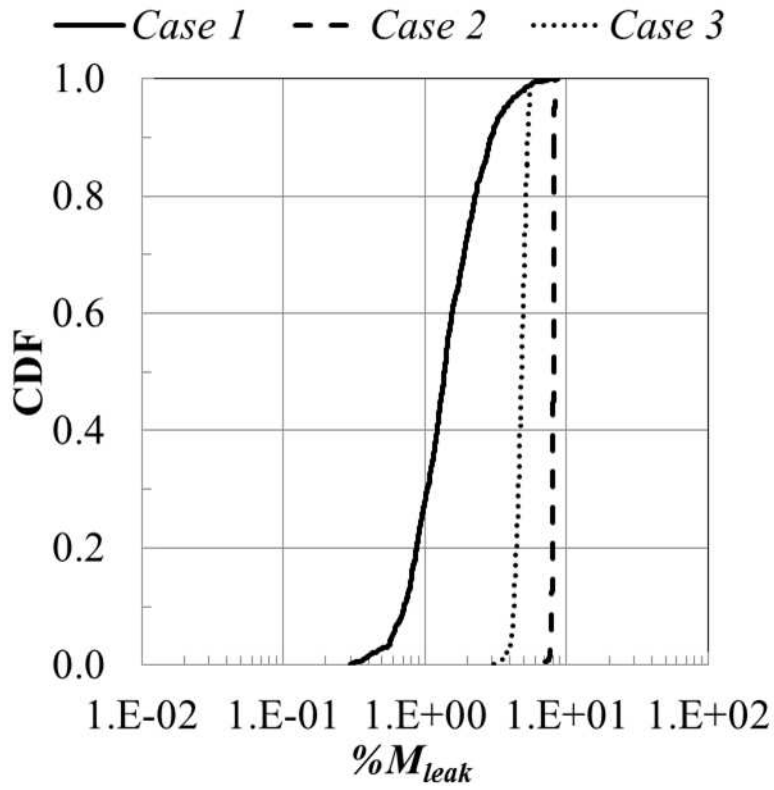


Figure 10. CDF of %CO₂ mass leakage associated with the uncertainty on passive well permeability. See Table 2 for descriptions of Case 1 – Case 3.

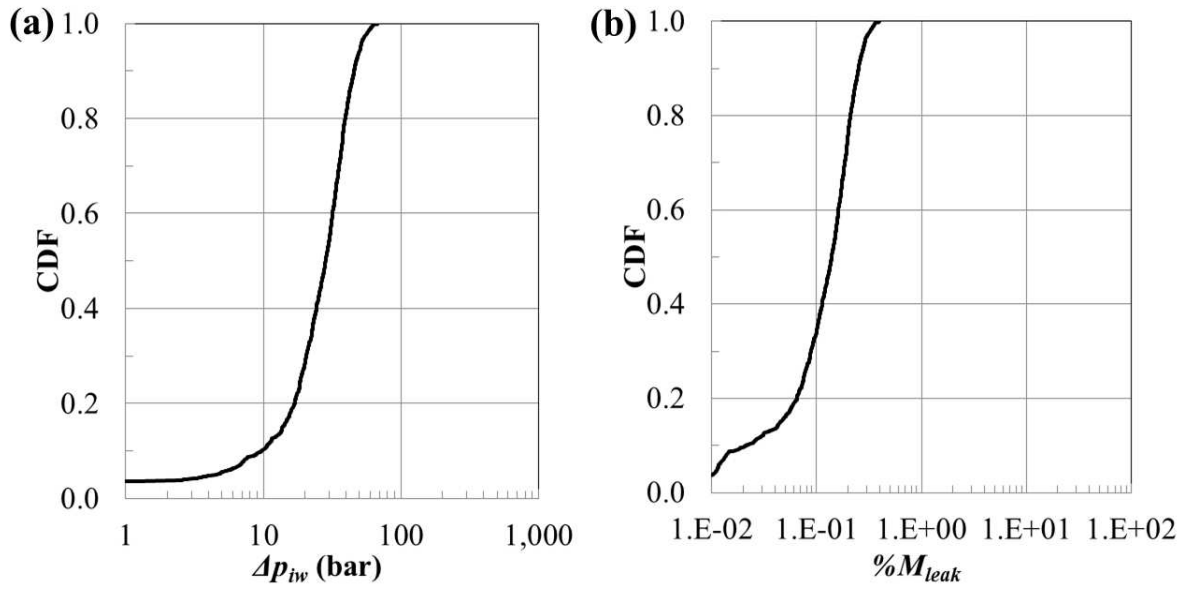


Figure 11. CDF of the (a) fluid overpressure nearby the injection well, and (b) %CO₂ mass leakage associated with the uncertainty on system compressibility.

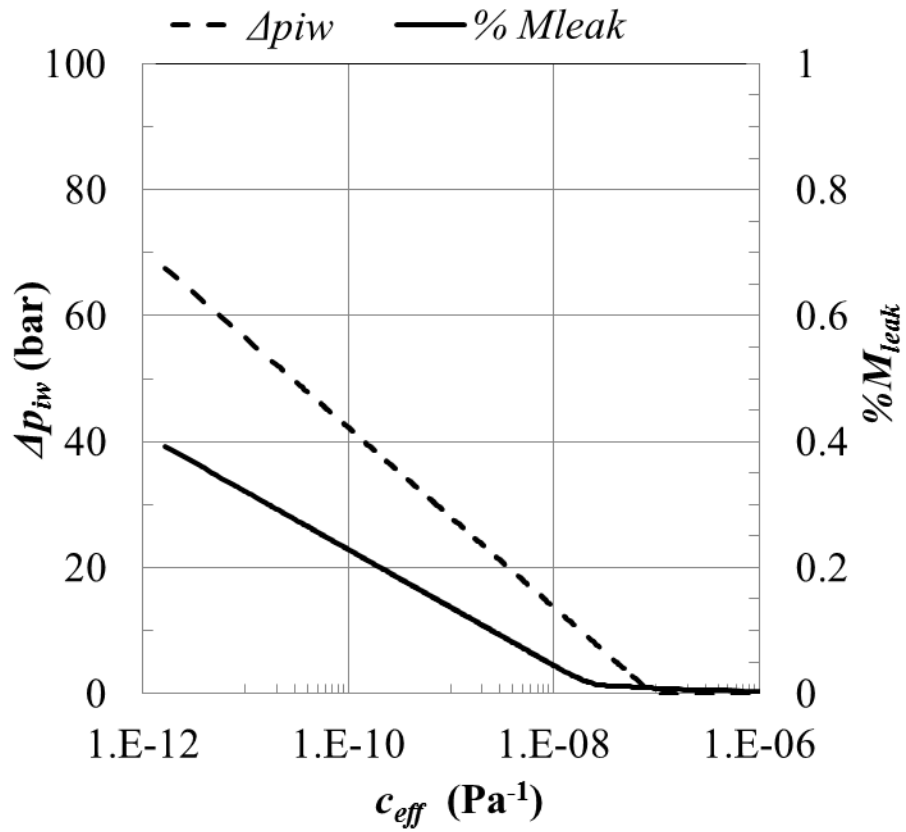


Figure 12. Fluid overpressure (left vertical axis) and %CO₂ mass leakage (right vertical axis) as functions of system compressibility.

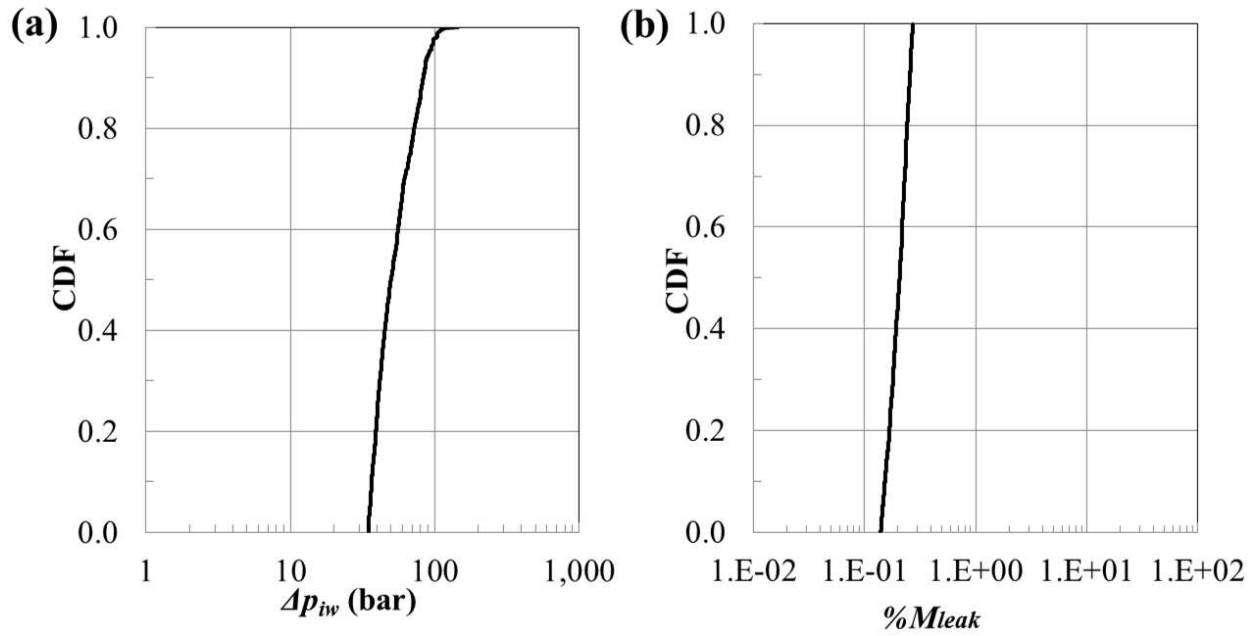


Figure 13. CDF of the (a) fluid overpressure nearby the injection well, and (b) %CO₂ mass leakage associated with the uncertainty on brine residual saturation.

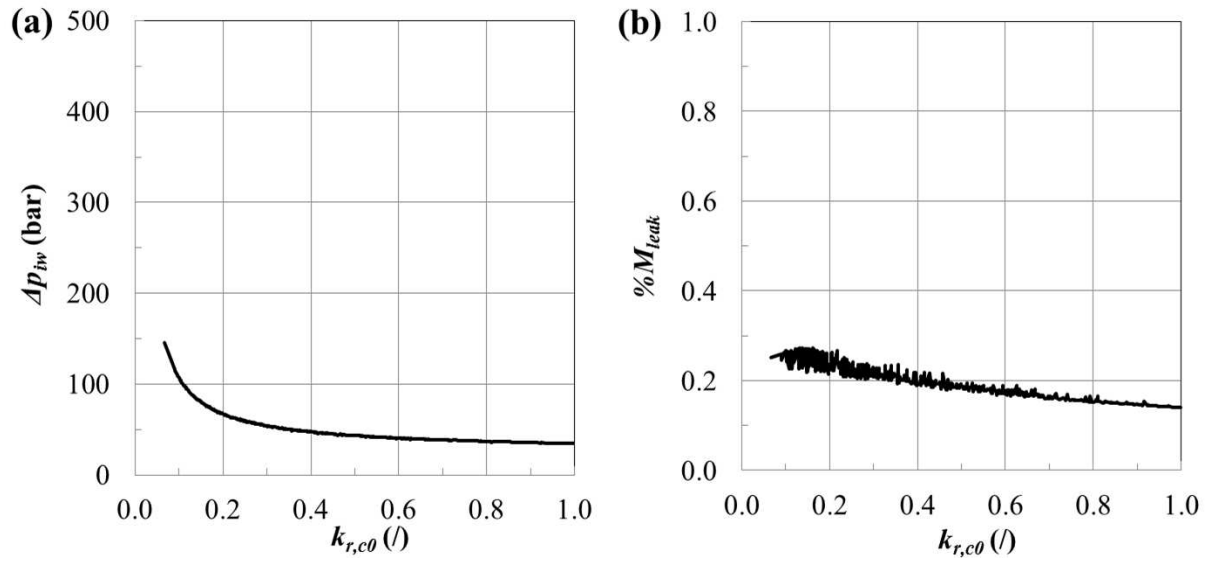


Figure 14. (a) Fluid overpressure nearby the injection well, and (b) %CO₂ mass leakage as a function of CO₂ end-point relative permeability.

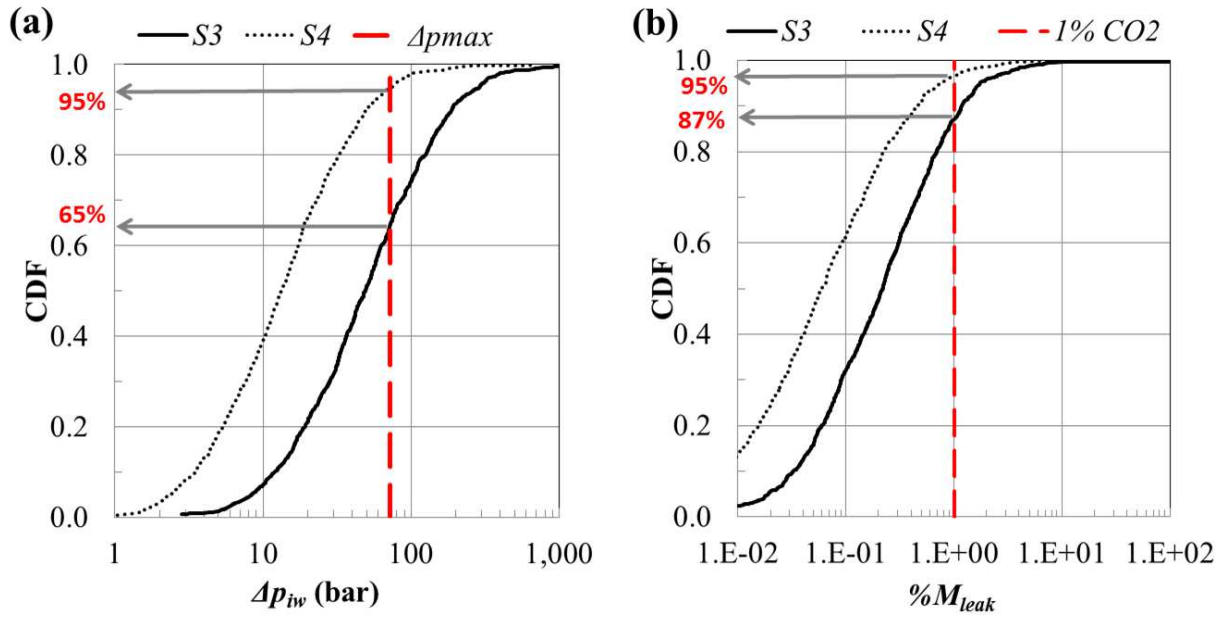


Figure 15. CDF of the (a) fluid overpressure nearby the injection well, and (b) %CO₂ mass leakage associated with the uncertainty on all uncertain parameters for scenarios S3 and S4. The vertical dashed line in (a) represents the maximum overpressure allowed at the injected formation and in (b) the %CO₂ mass leakage threshold.

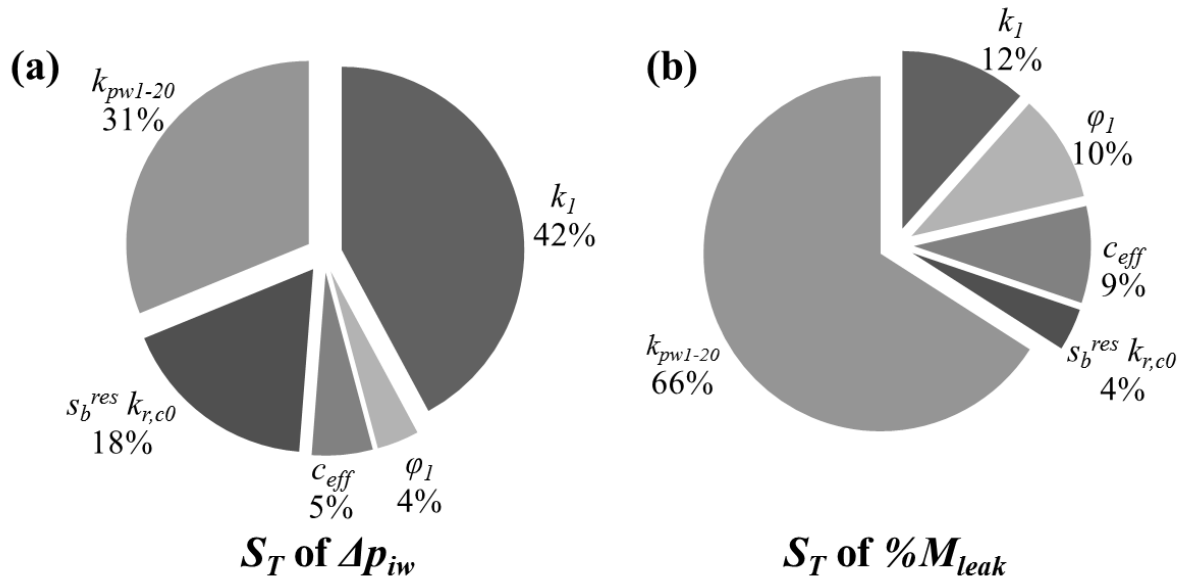


Figure 16. Extended FAST normalized total effect indices for: (a) maximum fluid overpressure in the vicinity of the injection well, and (b) %CO₂ mass leakage.